DAE−EKF−Based Nonlinear Predictive Control of Reactive Distillation Systems Exhibiting Input and Output Multiplicities

ARTICLE *in* INDUSTRIAL & ENGINEERING CHEMISTRY RESEARCH · SEPTEMBER 2013

Impact Factor: 2.59 · DOI: 10.1021/ie4004128

3 AUTHORS, INCLUDING:

J L Purohit
Dharmsinh Desai University
13 PUBLICATIONS **9** CITATIONS
SEE PROFILE

Sanjay Madhusudan Mahajani
Indian Institute of Technology Bombay
123 PUBLICATIONS **1,392** CITATIONS
SEE PROFILE

I&EC research
Industrial & Engineering Chemistry Research

Article

pubs.acs.org/IECR

DAE-EKF-Based Nonlinear Predictive Control of Reactive Distillation Systems Exhibiting Input and Output Multiplicities

Jalesh L. Purohit, Sachin C. Patwardhan,* and Sanjay M. Mahajani

Department of Chemical Engineering, Indian Institute of Technology, Bombay, Mumbai 400076, India

ABSTRACT: Reactive distillation (RD) has become one of the most important hybrid separation processes in recent times because of its economic and operational advantages. Reactive distillation systems, however, can exhibit complex input and output multiplicity behavior simultaneously in the desired operating region. Moreover, such a system is generally stiff and is typically modeled as a set of differential-algebraic equations. These two factors render the control of RD systems a challenging problem, particularly when the desirable operating point is unstable. In this work, an observer error feedback-based NMPC scheme has been developed for achieving offset-free control of RD systems modeled as DAEs. A recently developed version of the EKF for DAE systems (Mandela et al. *Chem. Eng. Sci.* **2010**, *65*, 4548−4556) was used to carry out state estimation. Because direct use of a DAE solver in the NMPC formulation can prove to be prohibitively computationally intensive and unsuitable for online implementation, a successive-linearization-based NMPC scheme (SLNMPC) was also developed. The effectiveness of the proposed control schemes is demonstrated by simulating servo and regulatory control problems associated with a hypothetical ideal RD column that exhibits input and output multiplicity behavior simultaneously at an unstable but economically desirable operating point. The servo and regulatory performances of the proposed SLNMPC scheme were also studied by simulating an industrial RD system involving MTBE synthesis. Analysis of the simulation results indicates that the proposed SLNMPC formulation provides an effective approach for handling control problems involving moderately large-magnitude servo and regulatory changes in the operation of RD systems. Moreover, the average computation time for the SLNMPC formulation was found to be quite small when compared with the sampling interval, which establishes the feasibility of implementing the SLNMPC scheme in real time.

1. INTRODUCTION

Reactive distillation (RD) has become one of the most important hybrid unit operations because of its advantages, such as complete conversion in equilibrium-limited reactions, heat integration through the utilization of the exothermic heat of reaction for volatilization, minimum waste generation, and economic benefits over the conventional reaction−separation sequence in the chemical process industries.[1] The interaction of reaction and separation in RD systems leads to a highly nonlinear behavior such as the occurrence of steady-state input and output multiplicities.[2] Process intensification often leads to extrema of the critical process parameters (such as conversion) inside the operating region,[3] which can give rise to input multiplicity behavior. Input multiplicities result if competing effects are present in nonlinear chemical processes and the steady-state gain matrix of the process becomes singular in the desired operating region.[4] Several authors have reported the existence of input and output multiplicities in RD systems.[5−7] A phenomenon associated with input multiplicity is change(s) in the sign(s) of the steady-state gain(s) in the desired operating region. As a consequence, the robustness of the linear controller with integral action is lost in the presence of input multiplicity.[8] Moreover, the input multiplicity behavior can pose significant difficulties even for a nonlinear control scheme.[9] The presence of output multiplicity behavior, on the other hand, leads to open-loop unstable dynamics at some of the multiple steady states. Al-Arfaj and Luyben[10] established that output multiplicity exists at constant reflux flow and constant reflux ratio for both low- and high-conversion designs of methyl acetate RD columns. The behavior of the process in the presence of output multiplicities depends on the process history, and the process output can be different for the same input move.[11] If it is desired to control the system at one of the unstable operating points, then designing a controller that stabilizes the system and achieves desired closed-loop performance is not an easy task. In fact, input and output multiplicities can occur simultaneously in some reactive distillation systems. Monroy-Loperena et al.[12] reported the simultaneous occurrence of input and output multiplicity behavior in the RD process for ethylene glycol synthesis. Controlling such an RD system is a challenging task. Difficulties in controller synthesis are further compounded by the fact that RD systems are often modeled as sets of coupled differential-algebraic equations (DAEs). As a consequence, most nonlinear state estimation and control approaches, which are typically developed for systems of ordinary differential equations (ODEs), have to be further modified to handle nonlinear algebraic constraints.

The implications of the occurrence of input multiplicity on the closed-loop performance of an ideal RD column regulated using multiloop proportional−integral−derivative (PID) controllers were investigated by Kumar and Kaishtha.[13] Whereas a conventional multiloop PID or linear multivariable control scheme, such as the robust multivariable controller developed by Volker et al.,[14] might be sufficient for carrying out regulation

Received: February 3, 2013
Revised: July 6, 2013
Accepted: August 6, 2013
Published: August 6, 2013

dx.doi.org/10.1021/ie4004128 | *Ind. Eng. Chem. Res.* 2013, 52, 13699−13716

at some desired operating point of an RD system, it is difficult to use these schemes when the controller is expected to implement large set-point changes that can significantly alter the local dynamic behavior of the process. The need to achieve tight control of a system exhibiting input and/or output multiplicities over a wide operating range necessitates the use of a nonlinear-model-based control scheme. Kumar and Daoutidis[15] studied the control problem associated with the ethylene glycol RD column, which is modeled as a DAE system. They designed a nonlinear input−output linearizing controller for the RD system and showed that the performance of the nonlinear controller is superior to that of linear multiloop controllers. Grüner et al.[16] developed an asymptotically exact input−output linearization-based nonlinear controller for a DAE system of relative order 1 and demonstrated its applicability to an RD column of industrial relevance. An implicit assumption in the development of such globally linearizing control schemes, however, is that elements of the steady-state gain matrix of the system do not change signs in the desired operating region.[17]

Over the past two decades, nonlinear model predictive control (NMPC) has emerged as a promising tool for solving complex and moderately large-scale industrial control problems.[18] This approach appears to be ideally suited for addressing the complexities that can arise in the control of RD columns as a result of the occurrence of steady-state multiplicities. However, applications of NMPC to control problems associated with RD systems are relatively scarce in the literature. Engell and Fernholz[3] developed an artificial-neural-network- (ANN-) based NMPC scheme and demonstrated that it is a promising approach for improving the performance of semibatch RD systems. Kawathekar and Riggs[19] and Venkateswarlu and Reddy[20] successfully used NMPC for the control of an ethyl acetate RD column. In both cases, however, no attempt was made to analyze the steady-state multiplicity behavior of the RD system or to address the difficulties that can arise in control as a result of the occurrence of such multiplicities. Moreover, NMPC approaches tailored to DAE systems are also available in the literature.[21−23] However, none of the reported applications of NMPC for the control of RD systems have included any attempt to address issues arising from the DAE structure of the modeling equations.

Model-based controllers, such as NMPC, are based on state feedback and require that reliable state observers be developed for estimating the states of the internal model. In particular, if the RD system under consideration exhibits output multiplicity behavior and if it is desired to control the system at one of the unstable operating points, then inclusion of a closed-loop observer becomes inevitable in the development of a model based control scheme. However, only a few reports have appeared in the literature on the application of state-estimation-based control schemes for RD columns. Grüner et al.[16] developed a nonlinear observer for use in combination with their feedback linearization-based control scheme. The proposed observer tuning procedure, however, was somewhat ad hoc and was based on certain specific characteristics of the temperature profiles of the system they considered. Olanrewaju and Al-Arfaj[24] used an extended Kalman filter (EKF) for inferential multiloop PI control of an ideal two-feed two-product RD column. They employed the conventional EKF formulation, which was developed for systems modeled as ODEs, by making some modifications in the RD model equations. As mentioned earlier, RD systems are often modeled as systems of DAEs and need a different treatment for state estimation.

A possible approach to solve the state estimation problem associated with DAE systems is to employ moving-horizon estimation (MHE), which can handle the algebraic constraints.[25] For a moderately large-dimensional system such as an RD column, using the conventional MHE formulation can prove to be quite computationally intensive and impractical for online implementation. Whereas the advanced-step MHE formulation of Zavala and Biegler[26] can alleviate the difficulties associated with online implementation, the estimation of the arrival cost in the MHE formulation needs to be carried out using a suitable nonlinear Bayesian DAE observer.[27] The topic of nonlinear Bayesian observers for systems modeled as DAEs is relatively unexplored. The extension of the Kalman filter to nonlinear DAE systems was developed by Becerra et al.[28] Their approach, however, can only accommodate measurements obtained from the differential states. This can prove to be a serious limitation for systems such as RD systems, for which the most readily available measurement is the temperature, which is determined using the algebraic vapor−liquid equilibrium (VLE) equations. To overcome this limitation, Mandela et al.[29] extended the work of Becerra et al.[28] to accommodate measurements obtained from either differential or algebraic states or both. They also showed how inequality constraints (i.e., bounds on estimated states) can be handled in the update step of their EKF formulation for the DAE systems (referred to as DAE-EKF in the rest of the text). Whereas the DAE-EKF formulation can be used for the estimation of the arrival cost in MHE, developing an NMPC scheme that is directly based on the DAE-EKF formulation of Mandela et al.[29] is a more attractive option in terms of online computational efficiency.

In this work, we developed a DAE-EKF-based NMPC formulation that is capable of handling control problems arising from the complex input and output multiplicity behavior of RD systems. To achieve offset-free closed-loop behavior, the observer error feedback approach developed by Srinivasrao et al.[9] and Huang et al.[30] was suitably modified and used to introduce integral action into the controller. In the NMPC formulation, the manipulated inputs are determined by solving a constrained nonlinear optimization problem at each sampling instant, which is a time-consuming step. If the average computation time for solving each optimization problem is comparable to or greater than the sampling time, then these computational delays deteriorate of control performance and can lead to stability problems.[31,32] Because mechanistic models for RD systems are of moderately large dimension and form stiff systems of equations owing to the differential-algebraic structure, the computation time is one of the main concerns in the development of an NMPC scheme for an RD column. Because the direct use of a DAE solver for carrying out predictions in the NMPC formulation leads to unacceptable average computation times for solving the optimization problem, similarly to Brengel and Seider,[33] we also developed a successive-linearization-based NMPC formulation (SLNMPC). The efficacy of the proposed NMPC scheme is demonstrated by solving control problem associated with an ideal reactive distillation column in which a prototypical quaternary reaction, a + b ↔ c + d, is carried out.[24] It is interesting to note that the economically attractive operating point of this system corresponds to an unstable steady state. Moreover, if it is desired to operate at the unstable point, then both output and input multiplicity exist simultaneously in the

operating region of interest. Motivated by the performance of SLNMPC for the hypothetical ideal RD column, the SLNMPC scheme was later used to solve servo and regulatory control problems associated with an industrially important RD system, namely, that used for the synthesis of methyl *tert*-butyl ether (MTBE).

This article is organized as follows: The DAE-EKF-based NMPC scheme and its simplification using successive linearization are described in section 2. Simulation case studies are presented and discussed in section 3. Finally, section 4 presents the main conclusions reached from the analysis of the simulation results.

2. DAE-EKF-BASED NMPC SCHEMES

2.1. Model for Plant Simulation and State Estimation. The reactive distillation systems under consideration can be represented in abstract form by the semiexplicit DAE system

$$\frac{d\mathbf{x}}{dt} = \mathbf{f}[\mathbf{x}(t), \mathbf{z}(t), \mathbf{m}(t), \mathbf{d}(t)] \tag{1}$$

$$\bar{\mathbf{0}} = \mathbf{G}[\mathbf{x}(t), \mathbf{z}(t)] \tag{2}$$

$$\mathbf{y}_T(t) = [\mathbf{C}_x \quad \mathbf{C}_z]\begin{bmatrix}\mathbf{x}(t)\\ \mathbf{z}(t)\end{bmatrix} \tag{3}$$

where $\mathbf{x} \in R^{n_d}$ represents the differential state variables, $\mathbf{z} \in R^{n_a}$ represents the algebraic state variables, $\mathbf{m} \in R^m$ represents the manipulated input variables, $\mathbf{d} \in R^d$ represents the unmeasured disturbance variables, and $\mathbf{y}_T \in R^r$ represents the true values of the measured output variables. The state estimation and predictions using this model were carried out under the following simplifying assumptions:

2.1.1. Assumption 1. The measurements, $\mathbf{y}_m(k)$, are obtained at a regular interval, h, and the measurement equation at the kth sampling instant is given by

$$\mathbf{y}_m(k) = [\mathbf{C}_x \quad \mathbf{C}_z]\begin{bmatrix}\mathbf{x}(k)\\ \mathbf{z}(k)\end{bmatrix} + \mathbf{v}(k) \tag{4}$$

Here, the measurement noise, $\mathbf{v}(k)$, is modeled as a zero-mean white-noise process with a Gaussian distribution, that is, $\mathbf{v}(k) \sim \mathcal{N}(\bar{\mathbf{0}}, \mathbf{R})$, where $\mathbf{R}$ represents the covariance matrix.

2.1.2. Assumption 2. The manipulated inputs are piecewise-constant over each sampling interval, that is

$$\mathbf{m}(t) = \mathbf{m}(k) \quad \text{for } t_k \le t < t_{k+1} = t_k + h$$

Further, the true values of the manipulated inputs ($\mathbf{m}$) are related to the known/computed values of the manipulated inputs ($\mathbf{u}$) as follows

$$\mathbf{m}(k) = \mathbf{u}(k) + \mathbf{w}_u(k) \tag{5}$$

where $\mathbf{w}_u(k) \in \mathbb{R}^m$ denotes an unknown disturbance in manipulated inputs such that $\mathbf{w}_u(k) \sim \mathcal{N}(\bar{\mathbf{0}}, \mathbf{Q}_u)$.

2.1.3. Assumption 3. The choice of the sampling interval is small enough that the variation of the unmeasured disturbances can be adequately approximated using piecewise-constant functions of the form

$$\mathbf{d}(k) = \bar{\mathbf{d}} + \mathbf{w}_d(k) \quad \text{for } t_k \le t < t_{k+1} = t_k + h$$

where $\mathbf{w}_d(k) \in \mathbb{R}^{d_u}$ denotes a disturbance in the unmeasured disturbance such that $\mathbf{w}_d(k) \sim \mathcal{N}(\bar{\mathbf{0}}, \mathbf{Q}_d)$ and $\bar{\mathbf{d}}$ represents the mean or steady-state value of the unmeasured disturbance at some desired operating point.

Thus, the plant is simulated by solving the following set of DAEs

$$\mathbf{x}(k+1) = \mathbf{x}(k) + \int_{kh}^{(k+1)h} \mathbf{f}[\mathbf{x}(\tau), \mathbf{z}(\tau), \mathbf{m}(k), \mathbf{d}(k)]\, d\tau \tag{6}$$

$$\bar{\mathbf{0}} = \mathbf{G}[\mathbf{x}(\tau), \mathbf{z}(\tau)] \tag{7}$$

using a suitable DAE solver. For the sake of convenience, the following notation is adopted to represent the DAE in eqs 6 and 7 in discrete form

$$\mathbf{x}(k) = \mathbf{F}[\mathbf{x}(k-1), \mathbf{z}(k-1), \mathbf{u}(k-1), \mathbf{w}(k-1)] \tag{8}$$

$$\bar{\mathbf{0}} = \mathbf{G}[\mathbf{x}(k), \mathbf{z}(k)] \tag{9}$$

where $\mathbf{w}(k)$ represents augmented state noise vector, that is

$$\mathbf{w}(k) = [\mathbf{w}_u{}^T(k)\ \mathbf{w}_d{}^T(k)]^T$$

with covariance matrices $\mathbf{Q} = \mathrm{diag}[\mathbf{Q}_u\ \mathbf{Q}_d]$.

2.2. NMPC Schemes Based on Observer Error Feedback. When it is desired to control the system under consideration at an unstable equilibrium point, it is important to develop the NMPC scheme using a closed-loop state estimator. In the present work, the state estimation for the semiexplicit DAE system given by eqs 8 and 9, together with the measurement model in eq 4, was carried out using the modified EKF algorithm proposed by Mandela et al.[29] A salient feature of this DAE-EKF formulation is that it accommodates measurements of algebraic states as well as differential states. This feature is particularly useful when the measured tray temperatures in the RD system under consideration are treated as algebraic states. The major steps in the estimation algorithm can be summarized as follows:

(1) The prediction step consists of computing predicted mean values of the differential and algebraic states. Thus, given estimates $(\hat{\mathbf{x}}(k-1|k-1), \hat{\mathbf{z}}(k-1|k-1))$, the prediction step is carried out using a suitable DAE solver

$$\hat{\mathbf{x}}(k|k-1) = \mathbf{F}[\hat{\mathbf{x}}(k-1|k-1), \hat{\mathbf{z}}(k-1|k-1), \mathbf{u}(k-1), \bar{\mathbf{0}}] \tag{10}$$

$$\bar{\mathbf{0}} = \mathbf{G}[\hat{\mathbf{x}}(k|k-1), \hat{\mathbf{z}}(k|k-1)] \tag{11}$$

to estimate $\hat{X}(k)(k|k-1)$.

(2) The predicted covariance matrix, $\mathbf{P}(k|k-1)$,of the augmented state estimates, $\hat{X}(k|k-1)$, is computed using a local linearization of the DAE model and used to compute the Kalman gain matrices (see Mandela et al.[29] for details).

(3) The observer gain matrices are used to compute updated state estimates

$$\begin{bmatrix}\hat{\mathbf{x}}(k|k)\\ \bar{\mathbf{z}}(k|k)\end{bmatrix} = \begin{bmatrix}\hat{\mathbf{x}}(k|k-1)\\ \hat{\mathbf{z}}(k|k-1)\end{bmatrix} + \begin{bmatrix}\mathbf{L}_x(k)\\ \mathbf{L}_z(k)\end{bmatrix}\mathbf{e}(k) \tag{12}$$

$$\mathbf{e}(k) = \mathbf{y}_m(k) - [\mathbf{C}_x \quad \mathbf{C}_z]\begin{bmatrix}\hat{\mathbf{x}}(k|k-1)\\ \hat{\mathbf{z}}(k|k-1)\end{bmatrix} \tag{13}$$

Because the updated differential and algebraic states, $(\hat{\mathbf{x}}(k|k), \tilde{\mathbf{z}}(k|k))$ together might not satisfy the differential equations, the

dx.doi.org/10.1021/ie4004128 | Ind. Eng. Chem. Res. 2013, 52, 13699−13716

algebraic states, $\hat{\mathbf{z}}(k|k)$ are recomputed using the differential states $\hat{\mathbf{x}}(k|k)$ by solving for

$$\bar{\mathbf{0}} = \mathbf{G}[\hat{\mathbf{x}}(k|k), \hat{\mathbf{z}}(k|k)] \tag{14}$$

3. NMPC SCHEMES BASED ON OBSERVER ERROR FEEDBACK

An observer error feedback NMPC scheme based on the extended Kalman filter (EKF)[30] can achieve offset-free closed-loop behavior when the measured outputs coincide with the controlled outputs. This approach, however, was developed for systems modeled using ODEs. Also, in general, the measured variables ($\mathbf{y}_m$) and the controlled output variables ($\mathbf{y}_c$) might not be identical. We consider a general case in which the controlled outputs are given as

$$\mathbf{y}_c(k) = [\mathbf{H}_x \quad \mathbf{H}_z]\begin{bmatrix}\mathbf{x}(k)\\ \mathbf{z}(k)\end{bmatrix} = \mathbf{H}_c\mathcal{X}(k)$$

where $\mathbf{y}_c(k) \in R^c$. The EKF-based NMPC scheme of Haung et al.[30] was modified in the present work to account for (a) systems modeled as DAEs and (b) distinct measured outputs ($\mathbf{y}_m$) and controlled variables ($\mathbf{y}_c$), that is, for inferential control.

3.1. Prediction of Future State and Output Trajectories. We consider two different approaches for the prediction of future state trajectories: using DAE solvers directly and using successive local linearization of the system of DAEs.

Direct Use of DAE Solvers. According to the first approach, similar to that of Haung et al.,[30] multistep predictions are carried out by explicitly using the observer errors for future predictions. Given a set of future manipulated input moves

$$\mathbf{U}_f = \{\mathbf{u}(k|k), \mathbf{u}(k+1|k), ..., \mathbf{u}(k+p-1|k)\} \tag{15}$$

it is proposed that the model predictions be generated as

$$\tilde{\mathbf{x}}(k+j+1|k) = \mathbf{F}[\tilde{\mathbf{x}}(k+j|k), \tilde{\mathbf{z}}(k+j|k), \mathbf{u}(k+j|k), \bar{\mathbf{0}}] + \mathbf{L}_x(k)\,\varepsilon(k) \tag{16}$$

$$\bar{\mathbf{0}} = \mathbf{G}[\tilde{\mathbf{x}}(k+j+1|k), \tilde{\mathbf{z}}(k+j+1|k)] \tag{17}$$

$$\varepsilon(k) = \mathbf{\Phi}_\varepsilon\varepsilon(k-1) + (\mathbf{I} - \mathbf{\Phi}_\varepsilon)\mathbf{e}(k|k-1) \tag{18}$$

$$\tilde{\mathbf{x}}(k|k) = \hat{\mathbf{x}}(k|k) \quad \text{and} \quad \tilde{\mathbf{z}}(k|k) = \hat{\mathbf{z}}(k|k) \tag{19}$$

for $j = 0, 1, 2, ..., p-1$, using any standard DAE solver. Here, $\varepsilon(k)$ represents filtered innovation, and the matrix $\mathbf{\Phi}_\varepsilon$ represents the error filter tuning parameter. Matrix $\mathbf{\Phi}_\varepsilon$ is parametrized as

$$\mathbf{\Phi}_\varepsilon = \mathrm{diag}[\alpha_1 \quad \alpha_2 \quad ... \quad \alpha_r]$$

where $0 \le \alpha_i < 1$ can be chosen to shape the regulatory response of the NMPC in the face of unmeasured input disturbances and model−plant mismatch.

Successive-Linearization-Based Predictions. The computations involved in the direct use of DAE solvers for generating predictions can prove to be an obstacle in the online implementation of NMPC for large-dimensional systems such as RD columns. A well-known remedy to this problem in the NMPC literature is to employ successive linearization (Brengel and Seider[33]). In this work , a suitably modified version of this approach was developed for systems modeled as DAEs and the observer error feedback scheme.

Consider the problem of generating future predictions using a continuous-time model

$$\frac{d\tilde{\mathbf{x}}}{dt} = \mathbf{f}[\tilde{\mathbf{x}}(t), \tilde{\mathbf{z}}(t), \mathbf{u}(t), \mathbf{d}(t)] \tag{20}$$

$$\bar{\mathbf{0}} = \mathbf{G}[\tilde{\mathbf{x}}(t), \tilde{\mathbf{z}}(t)] \tag{21}$$

with initial conditions

$$\tilde{\mathbf{x}}(t = kh) = \hat{\mathbf{x}}(k|k), \quad \mathbf{z}(t = kh) = \hat{\mathbf{z}}(k|k) \tag{22}$$

and with the future input sequence

$$\{\mathbf{u}(k|k), \mathbf{u}(k+1|k), ..., \mathbf{u}(k+N_p-1|k)\} \tag{23}$$

We first linearize the right-hand side of eq 20 in the neighborhood of the point

$$(\bullet) \equiv (\hat{\mathbf{x}}(k|k), \hat{\mathbf{z}}(k|k), \mathbf{u}(k-1), \bar{\mathbf{d}}) \tag{24}$$

as follows

$$\mathbf{f}[\tilde{\mathbf{x}}(t), \tilde{\mathbf{z}}(t), \mathbf{u}(t), \mathbf{d}(t)] \approx \mathbf{f}(k) + \mathcal{A}_x(k)\,\delta\tilde{\mathbf{x}}(t) + \mathcal{A}_z(k)\,\delta\tilde{\mathbf{z}}(t) + \mathcal{B}_u(k)\,\delta\mathbf{u}(t) + \mathcal{B}_d(k)\,\delta\mathbf{d}(t)$$

$$\delta\tilde{\mathbf{x}}(t) = \tilde{\mathbf{x}}(t) - \hat{\mathbf{x}}(k|k), \quad \delta\tilde{\mathbf{z}}(t) = \tilde{\mathbf{z}}(t) - \hat{\mathbf{z}}(k|k)$$

$$\delta\mathbf{u}(t) = \mathbf{u}(t) - \mathbf{u}(k-1), \quad \delta\mathbf{d}(t) = \mathbf{d}(t) - \bar{\mathbf{d}}$$

$$\mathbf{f}(k) = \mathbf{f}[\hat{\mathbf{x}}(k|k), \hat{\mathbf{z}}(k|k), \mathbf{u}(k-1), \bar{\mathbf{d}}]$$

$$\mathcal{A}_x(k) = \left[\frac{\partial\mathbf{f}}{\partial\mathbf{x}}\right]_{(\bullet)}, \quad \mathcal{A}_z(k) = \left[\frac{\partial\mathbf{f}}{\partial\mathbf{z}}\right]_{(\bullet)}$$

$$\mathcal{B}_u(k) = \left[\frac{\partial\mathbf{f}}{\partial\mathbf{u}}\right]_{(\bullet)}, \quad \mathcal{B}_d(k) = \left[\frac{\partial\mathbf{f}}{\partial\mathbf{d}}\right]_{(\bullet)}$$

$$\mathbf{G}[\tilde{\mathbf{x}}(t), \tilde{\mathbf{z}}(t), u(t), \mathbf{d}(t)] \approx \mathbf{g}(k) + \mathcal{G}_x(k)\;\delta\tilde{\mathbf{x}}(t) + \mathcal{G}_z(k)\,\delta\tilde{\mathbf{z}}(t) = \bar{\mathbf{0}}$$

$$\mathbf{g}(k) = \mathbf{G}[\hat{\mathbf{x}}(k|k), \hat{\mathbf{z}}(k|k)]$$

$$\mathcal{G}_x(k) = \left[\frac{\partial\mathbf{G}}{\partial\mathbf{x}}\right]_{(\bullet)}, \quad \mathcal{G}_z(k) = \left[\frac{\partial\mathbf{G}}{\partial\mathbf{z}}\right]_{(\bullet)}$$

$$\delta\tilde{\mathbf{z}}(t) = -[\mathcal{G}_z(k)]^{-1}[\mathbf{g}(k) + \mathcal{G}_x(k)\,\delta\tilde{\mathbf{x}}(t)]$$

From eq 9, it follows that $\mathbf{g}(k) = \bar{\mathbf{0}}$, and as a consequence, eq 20 can be locally approximated as

$$\frac{d\tilde{\mathbf{x}}}{dt} = \mathbf{f}(k) + \mathcal{A}(k)\,\delta\tilde{\mathbf{x}}(t) + \mathcal{B}_u(k)\,\delta\mathbf{u}(t) + \mathcal{B}_d(k)\,\delta\mathbf{d}(t) \tag{25}$$

$$\mathcal{A}(k) = \{\mathcal{A}_x(k) - \mathcal{A}_z(k)\,[\mathcal{G}_z(k)]^{-1}\,\mathcal{G}_x(k)\} \tag{26}$$

$$\tilde{\mathbf{x}}(t = kh) = \hat{\mathbf{x}}(k|k) \tag{27}$$

Equation 25 can be rearranged as

$$\frac{d\tilde{\mathbf{x}}}{dt} - \mathcal{A}(k)\,\tilde{\mathbf{x}}(t) = \mathcal{F}(k) + \mathcal{B}_u(k)\,\delta\mathbf{u}(t) + \mathcal{B}_d(k)\,\delta\mathbf{d}(t)$$

$$\mathcal{F}(k) = [\mathbf{f}(k) - \mathcal{A}(k)\,\hat{\mathbf{x}}(k|k)]$$

and then integrated over interval $t \in [t_k = kh, t_{k+1} = (k+1)h]$ using assumptions 1−3 (see sections 2.1.1−2.1.3). This results in the following discrete local approximation

dx.doi.org/10.1021/ie4004128 | Ind. Eng. Chem. Res. 2013, 52, 13699−13716

$$\tilde{\mathbf{x}}(k+1) = \Psi(k)\,\mathcal{F}(k) + \mathbf{\Phi}(k)\,\tilde{\mathbf{x}}(k) + \mathbf{\Gamma}_{\mathrm{u}}(k)\,\delta\mathbf{u}(k) + \mathbf{\Gamma}_{\mathrm{d}}(k)\,\mathbf{w}(k) \tag{28}$$

$$\delta\mathbf{z}(k+1) = -[\mathcal{G}_z(k)]^{-1}[\mathcal{G}_x(k)\,\delta\tilde{\mathbf{x}}(k+1)] \tag{29}$$

where

$$\Psi(k) = \int_0^h \exp[\mathbf{A}(k)\tau]\,\mathrm{d}\tau, \qquad \mathbf{\Phi}(i) = \exp[\mathbf{A}(k)h] \tag{30}$$

$$\mathbf{\Gamma}_{\mathrm{u}}(k) = \int_0^h \exp[\mathbf{A}(k)\tau]\mathcal{B}_{\mathrm{u}}(k)\,\mathrm{d}\tau \tag{31}$$

$$\mathbf{\Gamma}_{\mathrm{d}}(i) = \int_0^h \exp[\mathbf{A}(k)\tau]\mathcal{B}_{\mathrm{d}}(k)\,\mathrm{d}\tau \tag{32}$$

Given the set of future manipulated inputs, the model predictions are carried out using the local linear model as

$$\tilde{\mathbf{x}}(k+l+1|k) = \Psi(k)\,\mathcal{F}(k) + \mathbf{\Phi}(k)\,\hat{\mathbf{x}}(k+l|k) + \mathbf{\Gamma}_{\mathrm{m}}(k)\,\delta\mathbf{u}(k+l|k) + \mathbf{L}_x(k)\,\varepsilon(k) \tag{33}$$

$$\tilde{\mathbf{z}}(k+l+1|k) = \hat{\mathbf{z}}(k|k) - [\mathcal{G}_z(k)]^{-1}\{\mathcal{G}_x(k)[\tilde{\mathbf{x}}(k+l+1|k) - \hat{\mathbf{x}}(k|k)]\} \tag{34}$$

$$\delta\mathbf{u}(k+l|k) = \mathbf{u}(k+l|k) - \mathbf{u}(k-1) \tag{35}$$

$$l = 0, 1, 2, \ldots, N_{\mathrm{p}} - 1 \tag{36}$$

where $\varepsilon(k)$ is given by eq 18.

Predictions of Future Output Trajectories. If the controlled output variables $\mathbf{y}_{\mathrm{c}}(k)$ are not measured, then the output prediction assumes the form

$$\tilde{\mathbf{y}}_{\mathrm{c}}(k+j+1|k) = [\mathbf{H}_x \quad \mathbf{H}_z]\begin{bmatrix}\tilde{\mathbf{x}}(k+j+1|k)\\ \tilde{\mathbf{z}}(k+j+1|k)\end{bmatrix} \tag{37}$$

$$j = 0, 1, 2, \ldots, p-1$$

Alternatively, if $\mathbf{y}_{\mathrm{c}}(k)$ is a subset of $\mathbf{y}_{\mathrm{m}}(k)$, then the output predictions have the form

$$\tilde{\mathbf{y}}_{\mathrm{c}}(k+j+1|k) = [\mathbf{H}_x \quad \mathbf{H}_z]\begin{bmatrix}\tilde{\mathbf{x}}(k+j+1|k)\\ \tilde{\mathbf{z}}(k+j+1|k)\end{bmatrix} + \boldsymbol{\eta}(k) \tag{38}$$

$$\boldsymbol{\eta}(k) = \mathbf{\Phi}_\eta\boldsymbol{\eta}(k-1) + (\mathbf{I} - \mathbf{\Phi}_\eta)\mathbf{e}_{\mathrm{c}}(k|k) \tag{39}$$

$$\mathbf{e}_{\mathrm{c}}(k|k) = \mathbf{y}_{\mathrm{c}}(k) - [\mathbf{H}_x \quad \mathbf{H}_z]\begin{bmatrix}\hat{\mathbf{x}}(k|k)\\ \hat{\mathbf{z}}(k|k)\end{bmatrix} \tag{40}$$

for $j = 0, 1, 2, \ldots, p-1$. Here, $\boldsymbol{\eta}(k)$ represents the filtered update error, and matrix $\mathbf{\Phi}_\eta$ is the corresponding error filter tuning parameter. Matrix $\mathbf{\Phi}_\eta$ is parametrized as

$$\mathbf{\Phi}_\eta = \mathrm{diag}[\beta_1 \quad \beta_2 \quad \ldots \quad \beta_{\mathrm{c}}]$$

where $0 \le \beta_i < 1$ can be chosen to shape the regulatory response of the NMPC in the face of additive unmeasured disturbances in the controlled outputs.

3.2. NMPC Formulation. To achieve offset-free control, Huang et al.[30] recommended the inclusion of a target state in the NMPC objective function. The target state can be computed by solving the optimization problem

$$\min_{\bar{\mathbf{u}}(k)} [\mathbf{y}_{\mathrm{r}} - \bar{\mathbf{y}}_{\mathrm{c}}(k)]^{\mathrm{T}}\mathbf{W}_y[\mathbf{y}_{\mathrm{r}} - \bar{\mathbf{y}}_{\mathrm{c}}(k)] \tag{41}$$

subject to

$$\bar{\mathbf{x}}(k) = \mathbf{F}[\bar{\mathbf{x}}(k), \bar{\mathbf{z}}(k), \bar{\mathbf{u}}(k), \bar{\mathbf{0}}] + \mathbf{L}_x(k)\,\varepsilon(k) \tag{42}$$

$$\bar{\mathbf{0}} = \mathbf{G}[\bar{\mathbf{x}}(k), \bar{\mathbf{z}}(k)] \tag{43}$$

$$\bar{\mathbf{y}}_{\mathrm{c}}(k) = \mathbf{H}_{\mathrm{c}}\bar{\mathcal{X}}(k) + \boldsymbol{\eta}(k) \tag{44}$$

$$\mathbf{u}_{\mathrm{L}} \le \bar{\mathbf{u}}(k) \le \mathbf{u}_{\mathrm{H}} \tag{45}$$

When the controlled outputs are not measured directly, eq 44 is replaced by the equation

$$\bar{\mathbf{y}}_{\mathrm{c}}(k) = \mathbf{H}_{\mathrm{c}}\mathcal{X}(k)$$

It can be noted that inclusion of target states in the NMPC objective function does not guarantee offset-free behavior when the controlled outputs are not measured directly.

Given the model predictions and target state, NMPC is formulated as a constrained optimization problem over the moving time window $[k, k+N]$ as follows

$$\min_{\mathbf{U}_f} \sum_{j=1}^{N-1} [\mathbf{E}^{\mathrm{T}}(k+j|k)\mathbf{W}_{\mathrm{E}}\mathbf{E}(k+j|k)] \tag{46}$$

$$+\sum_{i=0}^{q-1} \Delta\mathbf{u}^{\mathrm{T}}(k+i|k)\mathbf{W}_{\Delta\mathrm{u}}\Delta\mathbf{u}(k+i|k) \tag{47}$$

$$+[\mathcal{X}(k+N) - \bar{\mathcal{X}}(k)]^{\mathrm{T}}\mathbf{W}_\infty[\mathcal{X}(k+N) - \bar{\mathcal{X}}(k)] \tag{48}$$

$$\mathbf{E}(k+j|k) = \tilde{\mathbf{y}}_{\mathrm{c}}(k+j|k) - \mathbf{y}_{\mathrm{r}} \tag{49}$$

$$\Delta\mathbf{u}(k+j|k) = \mathbf{u}(k+j|k) - \mathbf{u}(k+j-1|k) \tag{50}$$

$$\mathbf{y}_{\mathrm{r}} - \mathbf{C}_x\bar{\mathbf{x}} - \varepsilon(k) = \mathbf{0} \tag{51}$$

subject to

$$\mathbf{u}_{\mathrm{L}} \le \mathbf{u}(k+j|k) \le \mathbf{u}_{\mathrm{H}} \quad \text{for } j = 0, 1, \ldots, q-1 \tag{52}$$

$$\mathbf{u}(k+j|k) = \mathbf{u}(k+q-1|k) \quad \text{for } j = q, q+1, \ldots, p-1 \tag{53}$$

$$\mathbf{x}_{\mathrm{L}} \le \tilde{\mathbf{x}}(k+j|k) \le \mathbf{x}_{\mathrm{H}} \quad \text{for } j = 0, 1, \ldots, p-1 \tag{54}$$

where $\mathbf{y}_{\mathrm{r}}$ is the set point for the output; $\mathbf{W}_{\mathrm{E}}$, $\mathbf{W}_\infty$, and $\mathbf{W}_{\Delta\mathrm{u}}$ are positive-definite weighting matrices; N represents the prediction horizon; and q represents the control horizon. Depending on the approach used for the state trajectory predictions, the following two NMPC formulations arise: ideal NMPC, based on the direct use of the DAE solvers for predictions, and SLNMPC, based on successive linearization of the DAE system.

In the case of ideal NMPC, the resulting constrained optimization problem can be solved using any standard nonlinear programming (NLP) solver. On the other hand, the SLNMPC formulation can be transformed into a quadratic programming (QP) problem and solved much more efficiently using any standard QP solver. The controller is implemented in the moving-horizon framework. The first control move, $\mathbf{u}(k|k)$, is implemented, and the optimization problem is repeated at the next sampling instant.

dx.doi.org/10.1021/ie4004128 | Ind. Eng. Chem. Res. 2013, 52, 13699−13716

4. SIMULATION EXAMPLES

In this section, two reactive distillation systems are used to demonstrate the effectiveness of the proposed DAE-EKF-based NMPC formulation: an RD column with hypothetical reaction kinetics and ideal VLE[24] and an RD column for the production of methyl *tert*-butyl ether (MTBE)

The ideal system exhibits complex multiplicity behavior under certain configurations and thus poses a challenging control problem. The MTBE case study demonstrates the applicability of the proposed approach to a practical problem. To compare the performances of different NMPC schemes, we used the following two performance indices: a scalar performance index that is motivated by the NMPC objective function and defined as

$$I_{\mathrm{MPC}} \equiv \sum_{k=1}^{N_f} [\mathbf{y}_c(k) - \mathbf{y}_r(k)]^{\mathrm{T}} \mathbf{W}_{\mathrm{E}} [\mathbf{y}_c(k) - \mathbf{y}_r(k)] + \Delta \mathbf{u}^{\mathrm{T}}(k) \mathbf{W}_{\Delta u} \Delta \mathbf{u}(k)$$

where N_f denotes the number of samples in a simulation run, and the average time for the computation of $\mathbf{u}(k)$ on an Intel Core i7 processor (2.67 GHz, 4 GB of RAM).

4.1. Ideal Reactive Distillation System. First, an RD column with hypothetical reaction kinetics and ideal VLE[24] was chosen to demonstrate the efficacy of the proposed DAE-EKF-based NMPC formulation. The ideal RD column, with the quaternary hypothetical reaction a + b ↔ c + d, is illustrated in Figure 1. The reactive section contains N_{RX} trays, the rectifying section contains N_R trays, and the stripping section below the reactive section contains N_S trays. Reaction occurs only in the reactive section, where solid catalyst is present on trays. Pure reactant a enters the column on the first tray (N_S) of the reactive section, and pure reactant b enters the column on the last reactive stage ($N_S + N_{RX}$). The reactive distillation column has a total of N stages (excluding a reboiler and total condenser) and is numbered from bottom to the top. The light product c is removed as distillate, and the heavy product d is removed as bottoms. Various types of models, involving different levels of complexity, can be used to simulate the dynamics of the reactive distillation column. In this work, the simple and generic reactive distillation dynamic model studied by Al-Arfaj and Luyben[34] was considered. The kinetic and physical properties of the ideal RD system and the VLE parameters were taken from Al-Arfaj and Luyben.[34] The operating pressure of the column was 9 bar.

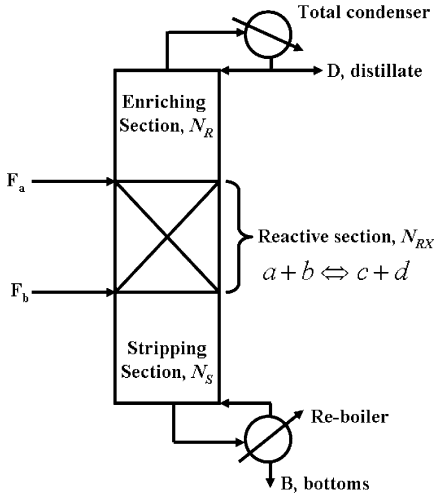

Figure 1. Ideal RD column: schematic representation.

For the RD system under consideration, the liquid compositions of all of the components on all stages, including the reboiler and condenser stages, and the molar holdups of the reboiler and condenser were considered as differential state variables, and the temperatures on all stages except the total condenser were considered as algebraic states. In eqs 1−3, $\mathbf{f}[\cdot]$ is the system function for the differential variables, and $\mathbf{G}[\cdot]$ represents the nonlinear VLE function that maps the vapor-phase concentrations to the stage temperatures and liquid-phase concentrations. To simulate the plant behavior or to carry out predictions with an observer/controller, the resulting set of DAEs was solved using an implicit Euler method with an integration interval of 1 s.

4.1.1. Steady-State Multiplicity. Nonlinear dynamic systems exhibit two types of multiplicities, namely, input multiplicity and output multiplicity. Input multiplicity is a phenomenon in which different values of input variable produce the same value of output variable in the steady-state solution, whereas output multiplicity is a phenomenon in which different steady-state solutions exist for the same value of an input variable. Whereas this ideal RD model considers a hypothetical reaction system, the resulting model is capable of revealing complex multiplicity behavior associated with a reaction−separation system. The existence of output multiplicity in an ideal RD column was reported by Kumar and Kaishtha[35] for a configuration with N_S = 5, N_{RX} = 10, and N_R = 5. In this work, bifurcation and control studies are presented for an ideal RD column with N_S = 7, N_{RX} = 6, N_R = 7, a reboiler, and a total condenser. It has been shown that the configuration under consideration is more economical for a stoichiometric feed.[36] In bifurcation studies, a continuation parameter is generally chosen from the set of inputs of the system. From the control perspective, a bifurcation study with respect to the manipulated input as the continuation parameter is important. The vapor boilup and reflux flow or reflux ratio are conventionally used as manipulated inputs to control the bottom and top compositions. In the present work, the vapor boilup was chosen as the continuation parameter, and the bifurcation study was carried out for both constant reflux flow and constant reflux ratio.

Bifurcation diagrams for the ideal RD column under constant reflux flow and under constant reflux ratio are shown in Figure 2. Figure 3 separately shows the steady-state multiplicity behavior at constant reflux flow rate for the bottom composition. Different steady-state operating conditions indicated in this figure are listed in Table 1. Unstable steady-state point A is the most desirable operating point, as the desired purity can be achieved at lower vapor boilup and, in turn, lower energy cost. It can be noted that, at the vapor boilup corresponding to operating steady state A (Figure 3), there are two stable steady states with higher and lower purities, which indicates the existence of output multiplicity at the corresponding value of the vapor boilup. The uncontrolled system will tend to settle at either of the two stable steady states if the inputs are held constant. The desired purity can also be achieved at higher vapor boilup rates corresponding to points B1 or B2 (Figure 3), which indicate the existence of input multiplicity. Thus, at the desired purity, both input and output multiplicities exist simultaneously, and as a consequence, control of this system at operating point A poses a challenging

dx.doi.org/10.1021/ie4004128 | Ind. Eng. Chem. Res. 2013, 52, 13699−13716

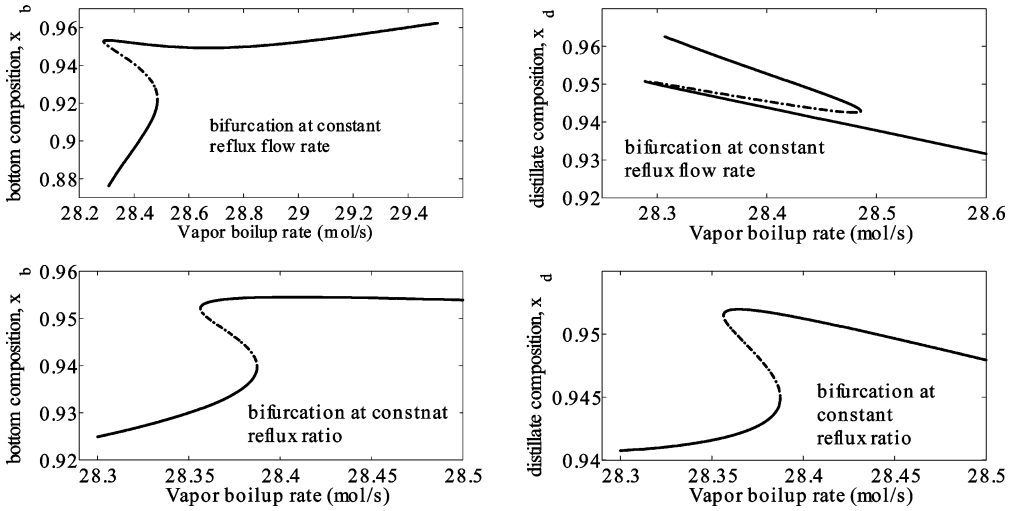

Figure 2. Steady-state multiplicity in an ideal RD 7/6/7 column at constant reflux flow rate and constant reflux ratio.

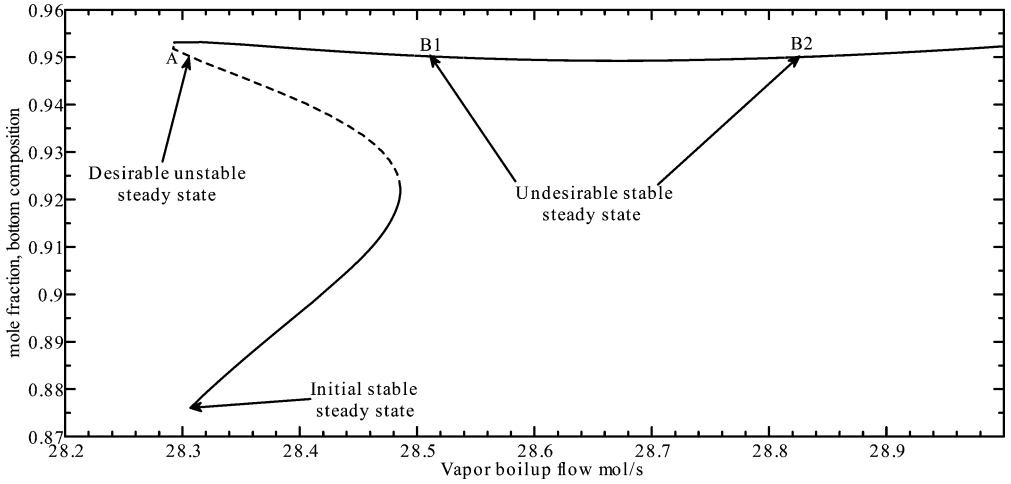

Figure 3. Steady-state multiplicity in an ideal RD 7/6/7 at constant reflux flow rate: bottom composition versus vapor boilup rate.

control problem. Moreover, in this design of an ideal RD column, output multiplicity was found to exist for constant reflux ratio as well (see Figure 2), so switching manipulation from reflux flow to reflux ratio cannot eliminate the multiplicity behavior.

4.1.2. Controller Configurations. In this work, we investigated a conventional control configuration and a configuration with stoichiometric balance.

In the conventional configuration, the reflux flow rate (r) and vapor boilup rate (V_s) are manipulated to control the distillate composition (x_d) and the bottom composition (x_b). The NMPC schemes (NMPC and SLNMPC) that manipulate (r, V_s) to control the estimated compositions (x_d, x_b) are referred to as conventional schemes.

Motivated by the control structures of Al-Arfaj and Luyben,[34] we also included the concentration of reactant a (x_a) at the feed stage of reactant a in the list of controlled outputs. Also, in addition to (r, V_s), the feed rate (F_a) of reactant a was also manipulated. It can be noted that controlling x_a is equivalent to maintaining the stoichiometric balance in the reactive section of the RD column. Thus, the NMPC schemes (NMPC and SLNMPC) that manipulate F_a together with (r, V_s) to control estimated (x_b, x_d, x_a) are referred to as stoichiometric schemes.

Note that perfect level controllers for reboiler level and condenser level were assumed to be present, as mentioned by Al-Arfaj and Luyben.[34] The lower and upper bound constraints used on manipulated inputs (r, V_s, F_a) were as follows

$$3.3 \leq r \leq 66 \text{ (mol/s)}$$

$$3 \leq V_s \leq 57 \text{ (mol/s)}$$

$$1.26 \leq F_a \leq 25.2 \text{ (mol/s)}$$

Depending on the availability of the measurements, two scenarios were considered: In scenario A, the servo control problem under the perfect model assumption, it was assumed that only temperatures were measured on 11 alternate stages starting from the reboiler stage. The molar holdups in the reboiler and condenser were also assumed to be measured variables. In scenario B, the regulatory control problem in the presence of unmeasured disturbances and/or model−plant mismatch, it was assumed that mole fractions x_b, x_d, and x_a were also measured, in addition to the measurements mentioned in scenario A. Inclusion of these additional measurements ensures offset-free closed-loop behavior in the presence of model−plant mismatch/unmeasured disturbances.

dx.doi.org/10.1021/ie4004128 | *Ind. Eng. Chem. Res.* 2013, 52, 13699−13716

Table 1. Ideal Distillation Column: Steady-State Operating Conditions[a]

	steady states			
	initial	A (desired)	B1	B2
	Flow Rates (mol/s)			
feed of reactant a	12.6	12.6	12.6	12.6
feed of reactant b	12.6	12.6	12.6	12.6
vapor boil-up	28.3072	**28.3072**	28.5195	28.8258
reflux	32.9454	32.9454	32.9454	32.9454
	Compositions (Mole Fraction)			
Bottom				
component a	0.0441	0.0021	0.0008	0.0006
component b	0.0779	0.0479	0.0492	0.0494
component c	0.0000	0.0000	0.0000	0.0000
component d	0.8762	**0.9500**	**0.9500**	**0.9500**
Feed Stage of F_a				
component a	0.5415	0.4307	0.3182	0.2925
component b	0.0525	0.0905	0.1547	0.1739
component c	0.0376	0.0433	0.0487	0.0491
component d	0.3685	0.4355	0.4783	0.4845
Distillate				
component a	0.0366	0.0479	0.0556	0.0648
component b	0.0008	0.0021	0.0079	0.0177
component c	0.9626	**0.9500**	0.9366	0.9175
component d	0.0000	0.0000	0.0000	0.0000

[a]The bold fonts represent the steady state values of inputs and outputs corresponding to point A in Figure 3.

A schematic representation of the EKF-based NMPC scheme is shown in Figure 4.

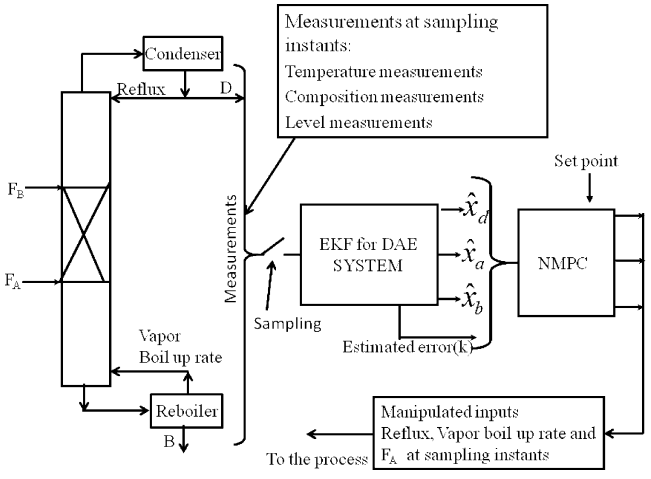

Figure 4. Block diagram of the EKF-based NMPC scheme for an RD column.

Each temperature measurement was assumed to be corrupted with a zero-mean, normally distributed white noise sequence with a standard deviation of 0.1 K. The holdup measurements were assumed to be corrupted with a zero-mean white noise with a standard deviation of 2 mol. It was assumed that the true values of the manipulated inputs ($\mathbf{m}$) were related to the computed values of the manipulated inputs ($\mathbf{u}$) as given by eq 5. The standard deviations (σ) for simulating the unmeasured disturbances were chosen to be 0.5% of the steady-state manipulated inputs ($\mathbf{u}$) corresponding to operating point A listed in Table 1. Thus, the covariance matrices used in the simulation were

$$\mathbf{Q}\,(\text{conventional scheme}) = \text{diag}[(0.1415)^2 \quad (0.1647)^2]$$

$$\mathbf{Q}\,(\text{stoichiometric scheme}) = \text{diag}[(0.1415)^2 \quad (0.1647)^2 \quad (0.063)^2]$$

The tuning parameters used in all NMPC formulations are listed in Table 2. Based on the recommendations made by

Table 2. NMPC Tuning Parameters

parameter	conventional	stoichiometric
prediction horizon, p	40	40
control horizon, q	4	4
sampling time, T_s	30 s	30 s
weighting matrix, W_E	$[0.1705, 1] \times 10^6$	$[1.4912, 8.7460, 1] \times 10^6$

Srinivasrao et al.,[9] the values of the filter tuning matrices $\mathbf{\Phi}_\varepsilon$ and $\mathbf{\Phi}_\eta$ in the proposed NMPC formulation were chosen to be

$$\mathbf{\Phi}_\varepsilon = 0.9\mathbf{I}_{n\times n} \quad \text{and} \quad \mathbf{\Phi}_\eta = 0.9\mathbf{I}_{r\times r}$$

These choices provide good robustness to the model−plant mismatch and reasonably fast recovery from the perturbations due to the unmeasured disturbances.

4.1.3. Set-Point Tracking Performance. Evaluation of the servo performance of the proposed NMPC schemes was carried out assuming that (a) the model is perfect and (b) only temperature measurements are available for state estimation and control. The set-point tracking problem addressed in the present work was to drive the ideal RD column from a lower stable steady state (initial steady state in Figure 3) to an unstable steady state (point A in Figure 3). Step changes were introduced simultaneously in both the top and bottom compositions of the top and bottom products. The output profiles of the bottom and top compositions in the absence of the measurement noise and stochastic disturbances are shown in Figure 5 for both NMPC schemes. The corresponding manipulated input profiles are presented in Figure 6. The two NMPC schemes settle the RD column at the desired values of the controlled outputs with almost equal settling times for both the stoichiometric and conventional configurations. However, closer examination of the manipulated input profiles (Figure 6) of the vapor boilup rate (V_s) and reflux flow rate (r) for both NMPC schemes reveals that, when the stoichiometric control configuration was used, the system settled at lower values of the inputs, corresponding to the unstable but economically attractive operating point A (Figure 3). The system inputs settled at their higher values corresponding to operating points similar to B1 or B2 (Figure 3) when the conventional control configuration was used. Figure 7 shows the manipulation of the feed rate of reactant a (F_a) to balance the reaction stoichiometry in the reactive section of the RD column through inventory control of reactant a. It can be noted that, in the conventional control configuration, x_a was not a controlled variable and, hence, the feed rate of reactant a, F_a, in the conventional control configuration remained constant at its steady-state value. On the other hand, F_a was manipulated in stoichiometric control configuration to maintain the stoichiometric balance in the reactive section.

The ideal RD system under consideration was found to exhibit very complex multiplicity behavior with simultaneous

dx.doi.org/10.1021/ie4004128 | Ind. Eng. Chem. Res. 2013, 52, 13699−13716

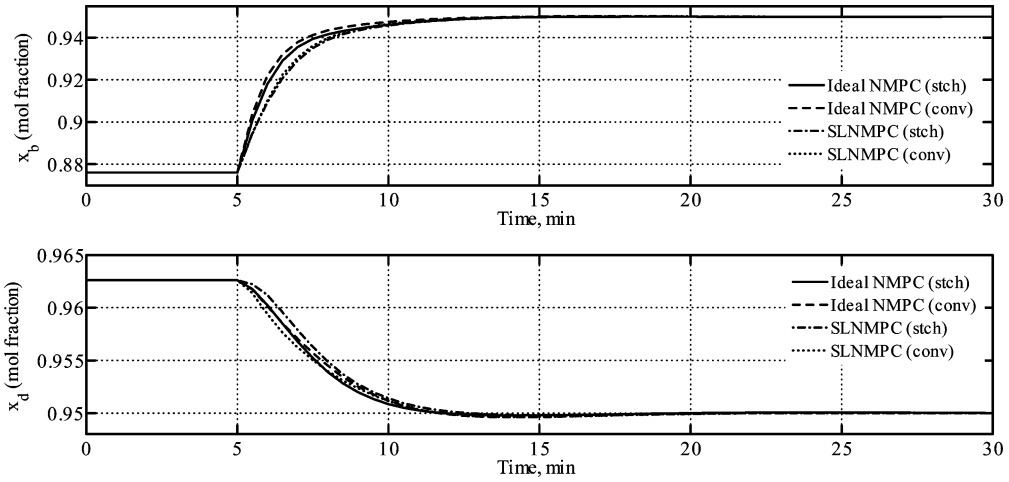

Figure 5. Profiles of controlled outputs (bottom composition of heavy product, x_b, and top composition of light product, x_d) for the set-point tracking problem.

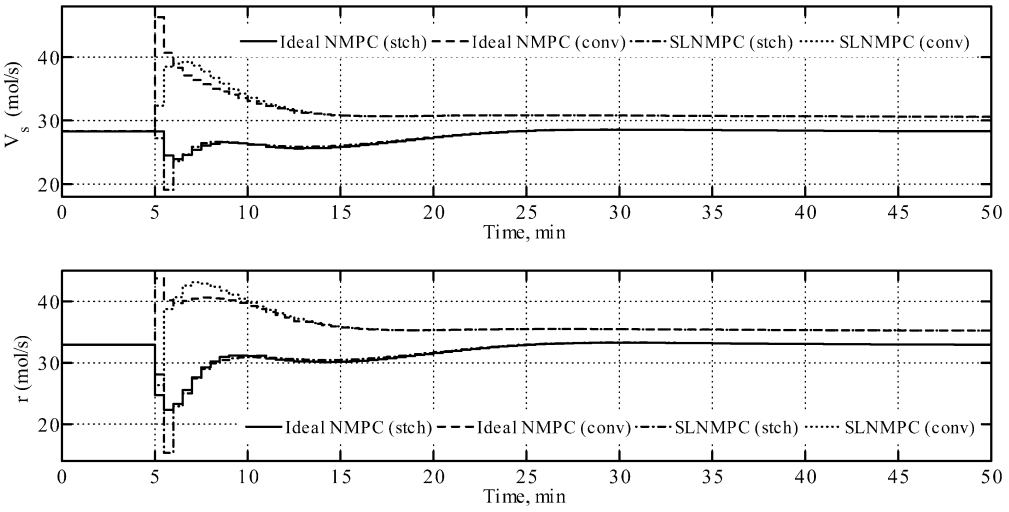

Figure 6. Profiles of manipulated inputs (vapor boilup rate, V_s, and reflux rate, r) for the set-point tracking problem.

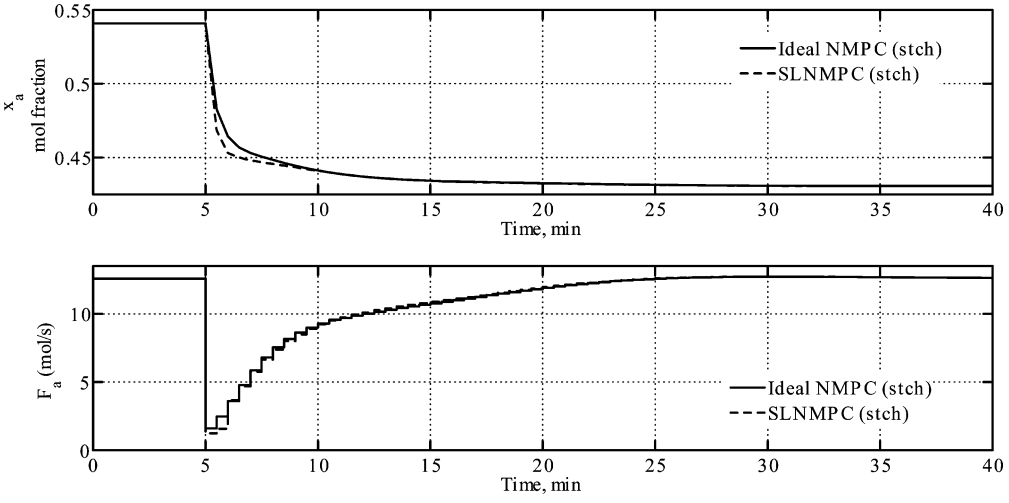

Figure 7. Profiles of controlled output (composition of reactant a on the feed stage, x_a) and manipulated input (F_a) for the stochiometric controller configuration for the set-point tracking problem.

input and output multiplicities with respect to the vapor boilup rate for the bottom composition as shown in Figure 3. In the bifurcation studies, the vapor boilup rate was chosen as the continuation parameter while all other parameters were kept constant, including F_a at 12.6 mol/s. The steady states corresponding to points A, B1, and B2 (Figure 3) indicate

dx.doi.org/10.1021/ie4004128 | Ind. Eng. Chem. Res. 2013, 52, 13699−13716

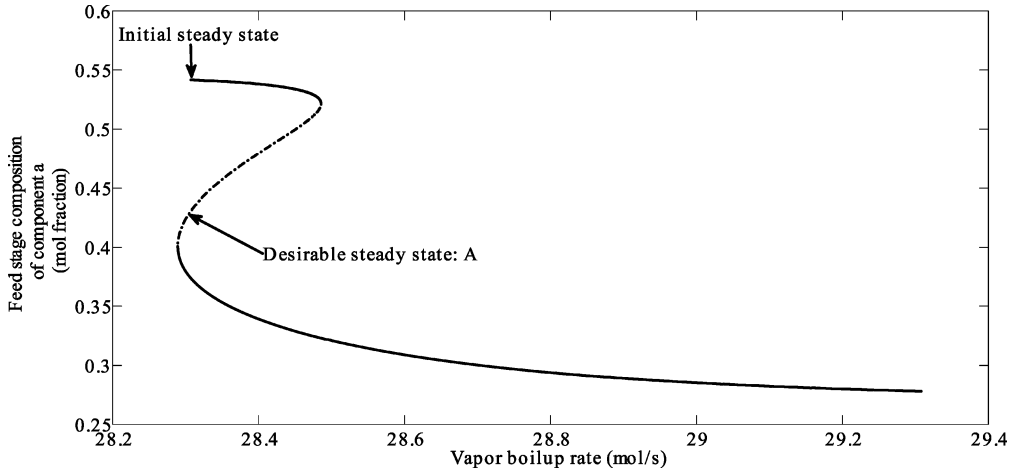

Figure 8. Steady-state multiplicity in an ideal RD 7/6/7 at constant reflux flow rate: feed-stage composition of reactant a versus vapor boilup rate.

Table 3. Performance Comparison between NMPC and SLNMPC

	ideal NMPC		SLNMPC	
	I_{MPC}	mean computational time (s)	I_{MPC}	mean computational time (s)
conventional	3.72×10^9	2166	3.73×10^9	3.73
stoichiometric	4.065×10^{12}	358.6	4.07×10^{12}	3.61

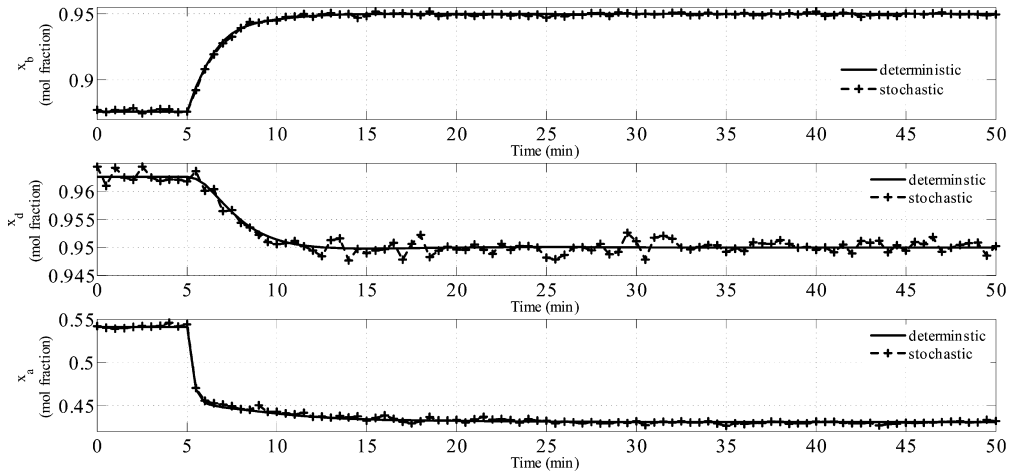

Figure 9. Profiles of controlled outputs (x_b, x_d, x_a): comparison between deterministic and stochastic simulation studies for the set-point tracking problem for the SLNMPC case.

the presence of input multiplicity with respect to the bottom composition at 95% purity. In addition, the system exhibited output multiplicity at point A, the desirable operating point. At the feed stage, on the other hand, the composition of reactant a (i.e., x_a) exhibited only output multiplicity with respect to the vapor boilup rate for F_a = 12.6 mol/s (see Figure 8 and Table 1). As a consequence, inclusion of a third variable in the set of controlled variables (i.e., x_a with a set point of 0.4307 mole fraction), together with the desired purity of 95% for the top and bottom compositions, in the stoichiometric control scheme ensured that the set point uniquely characterized point A. Thus, whereas F_a was manipulated during the transient, it finally settled at F_a = 12.6 mol/s, corresponding to the desirable operating point A. In the conventional scheme, on the other hand, whereas F_a remained constant at 12.6 mol/s, the vapor boilup rate (V_s) and the reflux flow rate (r), in their attempt to reach 95% purity with respect to the top and bottom compositions, settled at values other than those corresponding to point A. These results clearly indicate the importance of maintaining the stoichiometric balance in the reactive section to settle the RD column at the desired unstable steady state.

As can be expected from Figures 5 and 6, the performances of the ideal NMPC and SLNMPC schemes (see Table 3) were comparable when I_{MPC} was used as a performance measure. However, the mean computation time of ideal NMPC was very large with reference to the sampling interval (30 s), making it impractical for online implementation. The mean computation times for SLNMPC schemes, on the other hand, were significantly shorter than those of the ideal NMPC schemes and were also shorter than the sampling interval. Note that the average computation time for SLNMPC can be reduced further by employing a QP formulation of the SLNMPC problem instead of using sequential quadratic programming (SQP) (i.e., the fmincon function in MATLAB) that was used in the present work. Because the ideal NMPC formulation with a full nonlinear model did not show any significant advantage over

dx.doi.org/10.1021/ie4004128 | Ind. Eng. Chem. Res. 2013, 52, 13699−13716

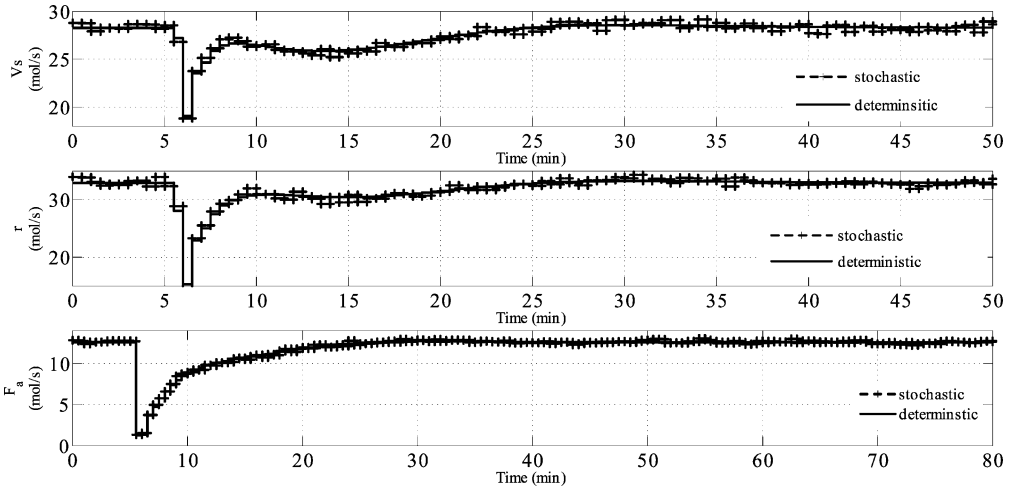

Figure 10. Profiles of manipulated inputs (V_s, r, F_a): comparison between deterministic and stochastic simulation studies for the set-point tracking problem for the SLNMPC case.

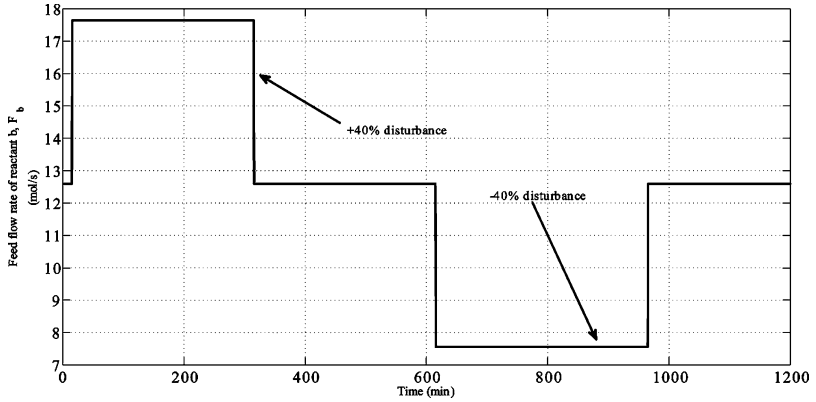

Figure 11. Disturbance in the feed rate (F_b) of reactant b.

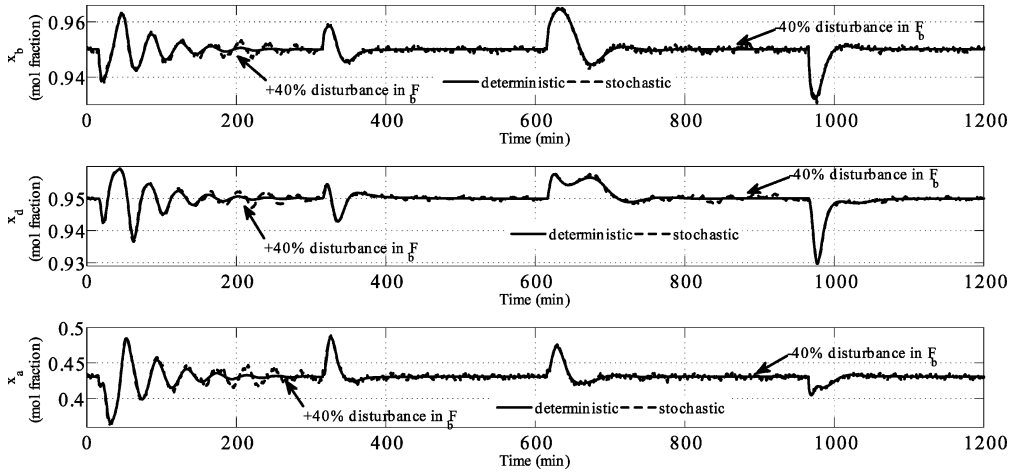

Figure 12. Profiles of controlled outputs for a ±40% disturbance in the feed rate (F_b) of reactant b.

the SLNMPC formulation for the ideal RD column under consideration, all subsequent simulation studies were carried out using the SLNMPC formulation.

In actual processes, process measurements are usually corrupted with noise, and the state dynamics is influenced by unmeasured inputs. Thus, it is important to evaluate the performance of the proposed observer-based SLNMPC schemes in the presence of unmeasured disturbances for the set-point tracking problem addressed in the present work, particularly when the final set-point change is an unstable steady state. Figures 9 and 10 compare the performances of SLNMPC for the servo problem with and without unknown disturbances and measurement noise. It is evident from the figures that the SLNMPC scheme with the stoichiometric configuration settled the RD column at the desired unstable

dx.doi.org/10.1021/ie4004128 | Ind. Eng. Chem. Res. 2013, 52, 13699−13716

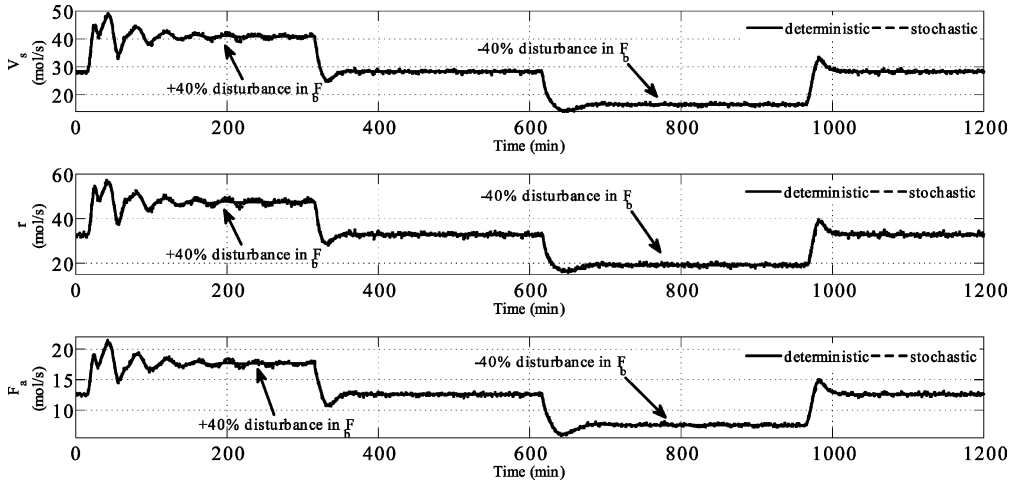

Figure 13. Profiles of manipulated inputs for a ±40% disturbance in the feed rate (F_b) of reactant b.

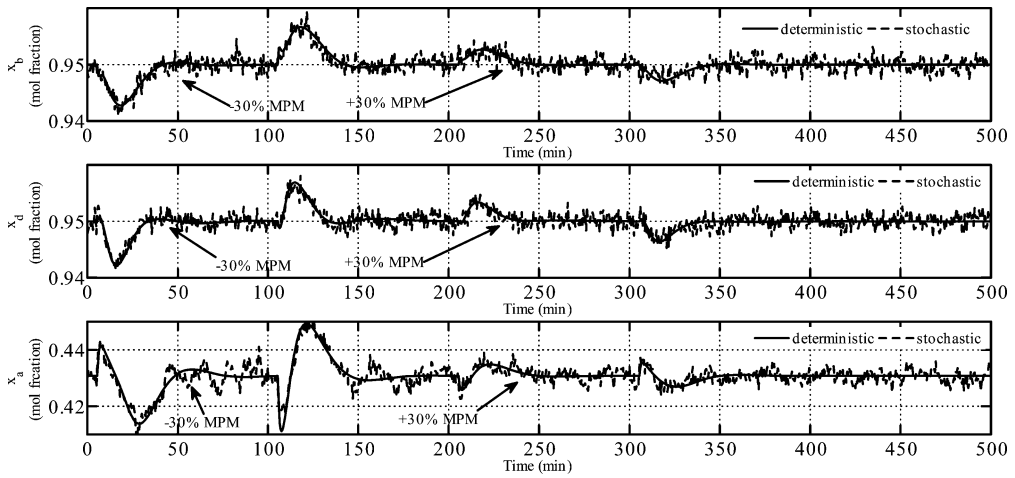

Figure 14. Profiles of controlled outputs in the presence of MPM (±30%) introduced in the rate constant.

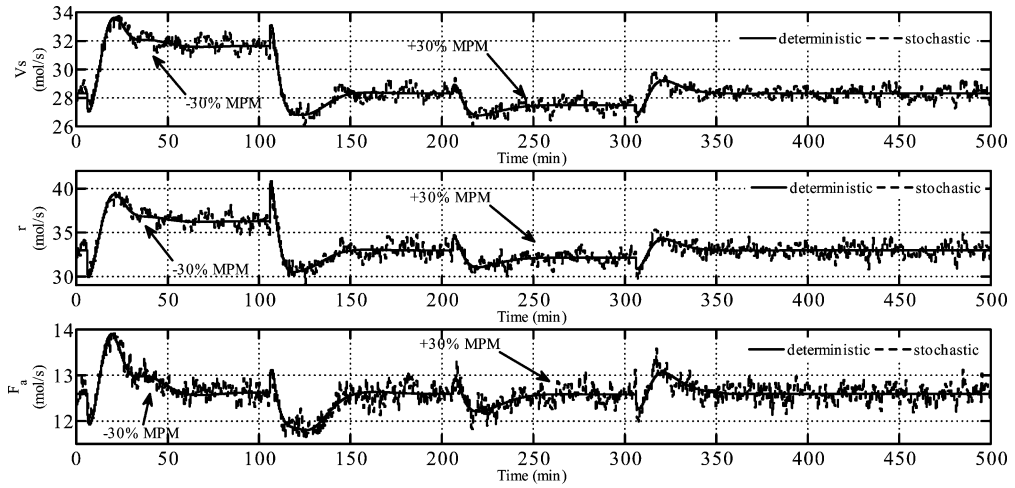

Figure 15. Profiles of manipulated inputs in the presence of MPM (±30%) introduced in the rate constant.

operating point even in the presence of measurement noise and unmeasured input disturbances.

4.1.4. Disturbance Rejection. From the set-point tracking performances, it was found that the SLNMPC scheme can be implemented online without compromising on the closed-loop performance. In particular, the stoichiometric control configuration settled the RD system at the economically attractive unstable steady state. Thus, the SLNMPC scheme with the stoichiometric control configuration was further investigated for the disturbance rejection problem in which ±40% (Figure 11) unmeasured disturbances in the feed rate (F_b) of reactant b was considered. In the servo control problem, it was assumed that

dx.doi.org/10.1021/ie4004128 | Ind. Eng. Chem. Res. 2013, 52, 13699−13716

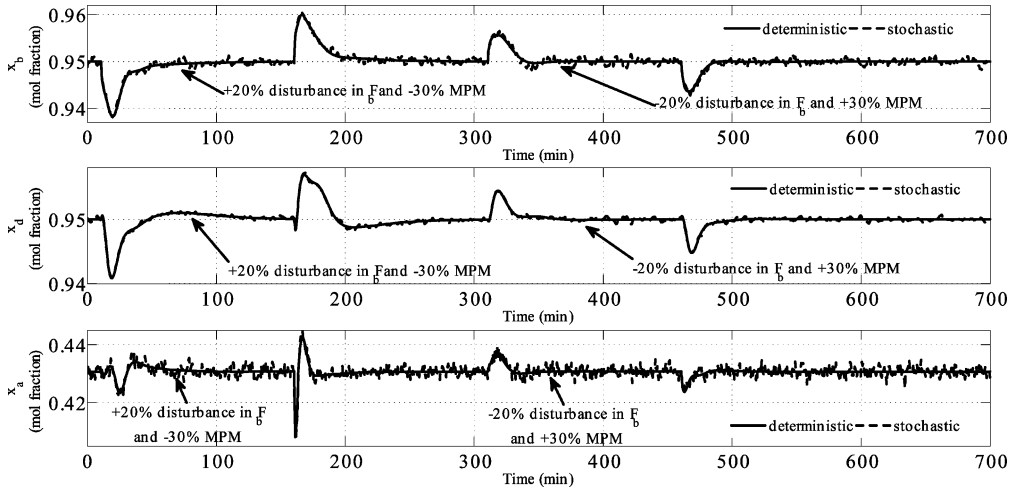

Figure 16. Profiles of controlled outputs: ±20% disturbance in F_b and in the presence of MPM (±30%) introduced in the rate constant.

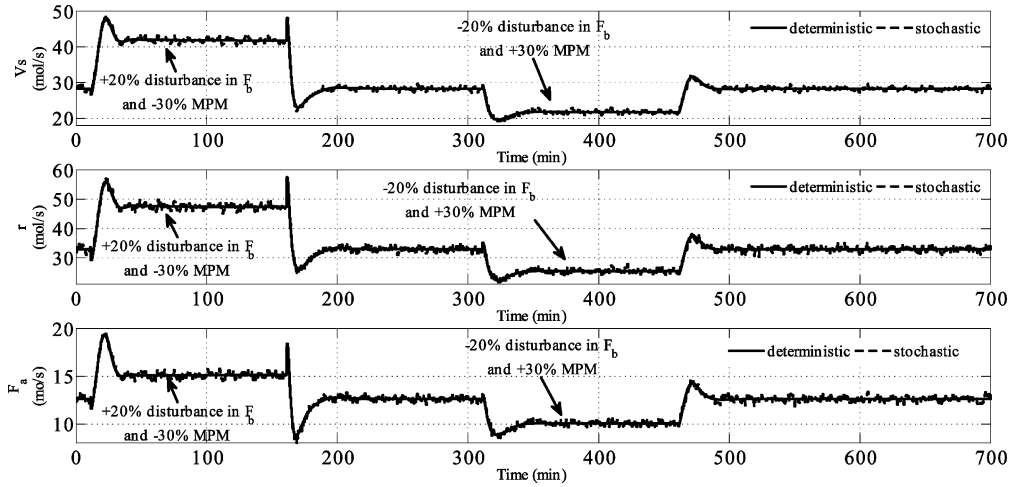

Figure 17. Profiles of manipulated inputs: ±20% disturbance in F_b and in the presence of MPM (±30%) introduced in the rate constant.

the controlled outputs were not measured and only state correction was used in the prediction equation. Because of the perfect model assumption, this resulted in offset-free inferential control. In the presence of model−plant mismatch and/or unmeasured disturbances, however, it becomes necessary to include measurements of the controlled outputs in the measurement set to achieve offset-free closed-loop behavior, that is, to switch to scenario B. Thus, the controlled outputs (x_b, x_d, x_a) were assumed to be measured in addition to the measured temperatures and two holdups. As a consequence, observer error feedback with state correction and output correction was used in the SLNMPC scheme for the disturbance and model−plant mismatch rejection problems. Each composition measurement was assumed to be corrupted with a zero-mean, normally distributed white noise sequence with a standard deviation 0.001 mole fraction. Figure 12 shows the output profiles of the controlled variables, and Figure 13 shows the manipulated input profiles for the disturbance rejection case considered in the present work for both the deterministic and stochastic simulations. It can be seen that the disturbances were rejected effectively even in the presence of noise.

4.1.5. Performance in the Presence of Model−Plant Mismatch. Development of a mathematical model from first principles is generally a very difficult task. It is also difficult to exactly estimate various physical and kinetic parameters in any chemical processes. This leads to model−plant mismatch (MPM), and it becomes necessary to study the performance of control scheme in the presence of MPM. In the present work, ±30% MPM was introduced in the values of the forward and backward reaction rate constants, and the performance of the SLNMPC was investigated. Figures 14 and 15 show the performance of the SLNMPC in the presence of MPM. It can be seen that the controlled outputs were effectively controlled at desired set point in the presence of MPM and stochastic disturbances.

In an actual process, disturbances in the inputs to the process occur simultaneously with MPM. Figures 16 and 17 show the performance of the SLNMPC for flow disturbances with MPM. It can be seen that SLNMPC effectively controlled the RD column at the desired set point when a step disturbance in flow and MPM occurred simultaneously. The closed-loop performance was not significantly different even when the measurement noise and unknown fluctuations in the manipulated inputs were added to the closed-loop simulation together with MPM and step disturbances.

4.2. MTBE RD Column. The second example is the production of methyl *tert*-butyl ether (MTBE) in an RD column. The MTBE RD column is an example of an RD system with nonideal VLE behavior and real reaction kinetics.

dx.doi.org/10.1021/ie4004128 | *Ind. Eng. Chem. Res.* 2013, 52, 13699−13716

Other than the nonideality, the main reason for including the MTBE column example is to stress that multiplicity scenarios that are qualitatively similar to those investigated using the ideal RD system can be encountered in systems of industrial relevance. This system exhibits output multiplicity behavior. It is important to study the problem of moving from an undesirable (low-conversion) steady state to a desirable (high-conversion) operating point in such real RD systems, particularly during startup operations. Sneesby et al.[37] investigated the various alternatives for driving the MTBE RD column from the undesirable steady state to the desirable steady state. They concluded that it is difficult for a linear controller to drive the MTBE RD column from an undesirable to a desirable operating point and recommend use of an adaptive controller for achieving such a transition.

In this simulation study, the system was first moved from the initial undesirable steady state to the middle unstable steady state. Whereas the middle unstable steady state of the MTBE column is not interesting from the operation point of view, the simulation study demonstrated that it is possible to stabilize the system at the unstable steady state even in the face of stochastic disturbances. With reference to the regulatory problem in the face of step disturbances investigated in the present work, it can be noted that oscillations were reported by Wang et al.[38] using a linear PI controller in an MTBE RD column for a similar disturbance rejection problem. In the present work, the RD model considered was a simplified model and not the same as that used by Wang et al.[38] However, from the control point of view, the DAE-based SLNMPC proposed in the present work effectively rejected qualitatively similar step disturbances.

MTBE is produced (Figure 18) by the etherification of isobutene with methanol in the presence of a strong acid

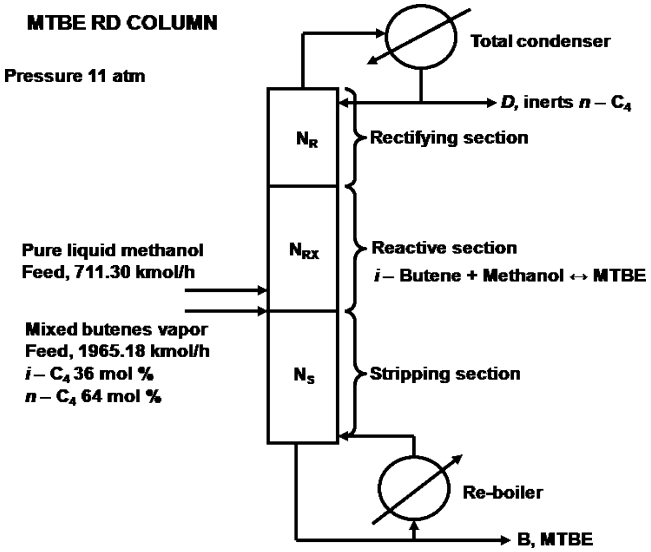

Figure 18. MTBE RD column: schematic diagram.

catalyst. Usually, butene feed also consists of *n*-butene, which does not take part in the reaction and remains in the system as an inert component. The primary objective of the RD column is to offer high-purity MTBE product from the bottoms and a distillate product containing high-purity *n*-butene. The feed flow rates and feed compositions were obtained from Singh et al.[6] The reaction kinetic data were taken from Rehfinger and Hoffman,[39] and the Wilson VLE model was used for nonidealities of the liquid phase. The dynamic RD model used in the MTBE case was the same as that used for the ideal RD column with constant flow rates in the nonreactive section, whereas in the reactive section, the flow rates varied because of the effect of the exothermic heat of reaction. The ideal VLE model was replaced with the nonideal VLE Wilson model, and the reaction kinetics was replaced with MTBE reaction kinetics.[39] The numbers of stages were kept as $N_S = 10$, $N_{RX} = 6$, and $N_R = 3$. The mixed butene feed was fed on stage $N_S + 1$, and methanol was fed on stage $N_S + 2$. The latent heat of vaporization and heat of reaction were assumed to be constant at 29000 and −37700 kJ/kmol, respectively. The catalyst weight on the reactive stages were taken as 1800 kg.

4.2.1. Steady-State Multiplicity in an MTBE RD Column. The MTBE RD column considered in the present work exhibits steady-state multiplicity (see Figure 19) when the vapor boilup rate is chosen as the continuation parameter and the reflux rate is kept constant. The desirable steady-state values for the MTBE RD column are listed in Table 4. The upper steady state is desirable with 99% MTBE purity in the bottom product. The corresponding top product contains 90% inert *n*-C_4. Multiple steady-state data are listed in Table 5.

4.2.2. Manipulated Inputs. For the MTBE RD column, the reflux flow rate (r) and vapor boilup rate (V_s) were manipulated to control the inert *n*-C_4 composition in the distillate (x_d) and the MTBE composition in the bottoms (x_b). Motivated by the MTBE RD column control structures of Luyben and Yu,[40] the concentration of methanol ($x_{methanol}$) reactant on the feed stage of methanol was also included in the list of controlled outputs, and the molar feed ratio of methanol feed to mixed butene feed was additionally treated as a manipulated input. Thus, the feed rate of mixed butenes was kept fixed, and the feed rate of methanol was manipulated through feed ratio control. The manipulation of the feed rate of one of the reactants was carried out to balance the stoichiometric requirements of the reactants in the reactive section. The lower and upper bound constraints used on the manipulated inputs $[r, V_s, (F_{methanol}/F_{butenes})]$ were

$$3350 \le r \le 33500 \text{ (kmol/h)}$$

$$3070 \le V_s \le 30700 \text{ (kmol/h)}$$

$$0.2 \le (F_{methanol}/F_{butenes}) \le 0.6$$

A total of 13 temperature measurements and 3 composition measurements of the controlled states were assumed to be available. Each temperature measurement was assumed to be corrupted with a zero-mean, normally distributed white noise sequence with a standard deviation of 0.1 K. The composition measurements of the controlled states were assumed to be corrupted with a zero-mean, normally distributed white noise sequence with a standard deviation of 0.001 mole fraction. The standard deviations (σ) for simulating the unmeasured disturbances were kept at 0.5% of the steady-state manipulated inputs ($\mathbf{u}$) listed in Table 4. Thus, the covariance of signal $\mathbf{w}_u$ (i.e., σ^2) is given as

$$\mathbf{Q} = \text{diag}[(76.75)^2 \quad (83.75)^2 \quad (0.0018)^2]$$

The NMPC tuning parameters are listed in Table 6. The filter tuning matrices $\mathbf{\Phi}_\varepsilon$ and $\mathbf{\Phi}_\eta$ were kept the same as for the ideal RD simulation example.

4.2.3. Set-Point Tracking. The servo performance of SLNMPC for the MTBE RD column was carried out under the assumption of a perfect model. For state estimation and

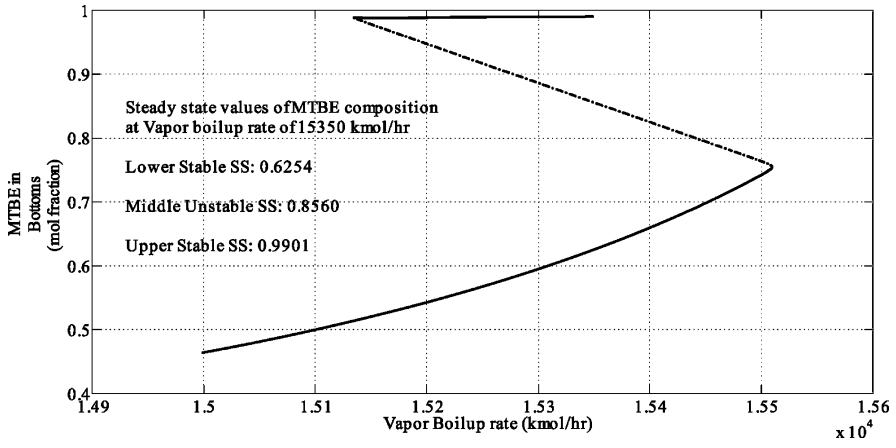

Figure 19. Steady-state multiplicity in an MTBE RD column.

Table 4. Steady-State Data for the MTBE RD Column

parameter	value
Column Specifications	
pressure (bar)	11
no. of trays	
stripping section, N_S	10
reactive section, N_{RX}	6
rectifying section, N_R	3
Flow Rates (kmol/h)	
feed of methanol	711.3
feed of butene mixture	1965.18
vapor boil-up	15350
reflux	16750
distillate	1394.4
bottoms	644.2
methanol/butenes molar feed ratio	0.3620
Distillate Composition	
i-C_4	0.0499
methanol	0.0481
MTBE	0.0000
n-C_4	0.9020
Bottoms Composition	
i-C_4	0.0000
methanol	0.0099
MTBE	0.9901
n-C_4	0.0000

Table 5. Multiple Steady-State Data for the MTBE RD Column

	steady states		
	lower	middle	upper
MTBE in bottoms (mole fraction)	0.6254	0.8560	0.9901
n-C_4 in distillate (mole fraction)	0.8702	0.9273	0.9020
methanol on feed stage (mole fraction)	0.0207	0.0307	0.8436
Bottoms (kmol/h)	865.9	711.04	644.32
Distillate (kmol/h)	1269.5	1356.7	1394.4

control, measurements of temperatures and concentrations of controlled states were assumed to be available. The set-point tracking problem addressed here was to drive the MTBE RD column from a lower stable steady state (Figure 19) to a middle unstable steady state and later to the stable steady state corresponding to an MTBE purity of 99%. Whereas the final steady state is desirable from an economic point of view, moving the system to the unstable middle state was of academic interest in the present work. A sequence of step changes was introduced simultaneously in all three controlled states. The output profiles of the MTBE composition in the bottoms and the n-C_4 composition in the top in the presence of measurement noise and stochastic disturbances are shown in Figure 20. The methanol inventory on the feed stage of methanol was also controlled (Figure 21) to maintain the stoichiometric balance by manipulating the feed ratio. The corresponding manipulated input profiles are presented in Figure 21. The feed rate of methanol (Figure 21) was controlled by manipulation of the feed ratio. It can be seen from these results that SLNMPC settled the MTBE RD column at an unstable steady state under stochastic disturbances and measurement noise. The SLNMPC later swiftly moved the process to the high-purity operating point.

Table 6. NMPC Tuning Parameters for the MTBE RD Column

parameter	value
prediction horizon, p	100
control horizon, q	6
sampling time, T_s	4 min
weighting matrix, W_E	$[1, 0.1, 2.5] \times 10^7$

4.2.4. Disturbance Rejection. The performance of the SLNMPC scheme on the MTBE RD column at the desirable upper operating steady state with 99% MTBE purity in the bottoms (see Figure 19) for ±20% unmeasured disturbances (Figure 22) in the feed rate of mixed butenes was investigated. Figure 23 shows the output profiles of the controlled variables, and Figure 24 shows the manipulated input profiles for the disturbance rejection case considered in the present work for stochastic simulations. It can be seen that these moderately large changes in unmeasured disturbances were rejected effectively without causing noticeable changes in the MTBE mole fraction in the bottoms composition. The response of the closed-loop system in the presence of MPM was qualitatively similar to that of the ideal RD column and is not included separately.

5. CONCLUSIONS

Reactive distillation (RD) systems can exhibit complex input and output multiplicity behavior simultaneously in the desired

dx.doi.org/10.1021/ie4004128 | Ind. Eng. Chem. Res. 2013, 52, 13699−13716

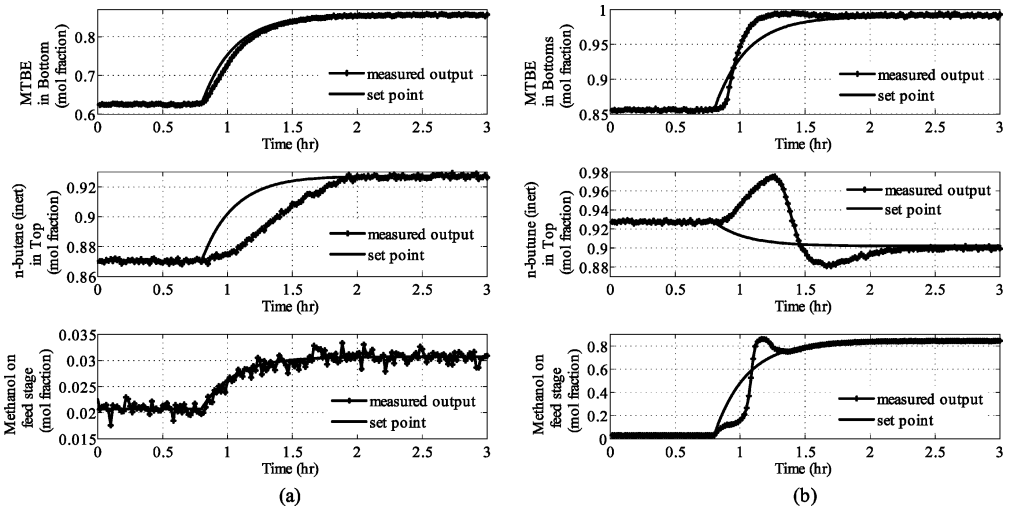

Figure 20. Profiles of controlled outputs for the set-point tracking problem under stochastic conditions: (a) from the lower steady state to the middle steady state and (b) from the middle steady state to the upper steady state.

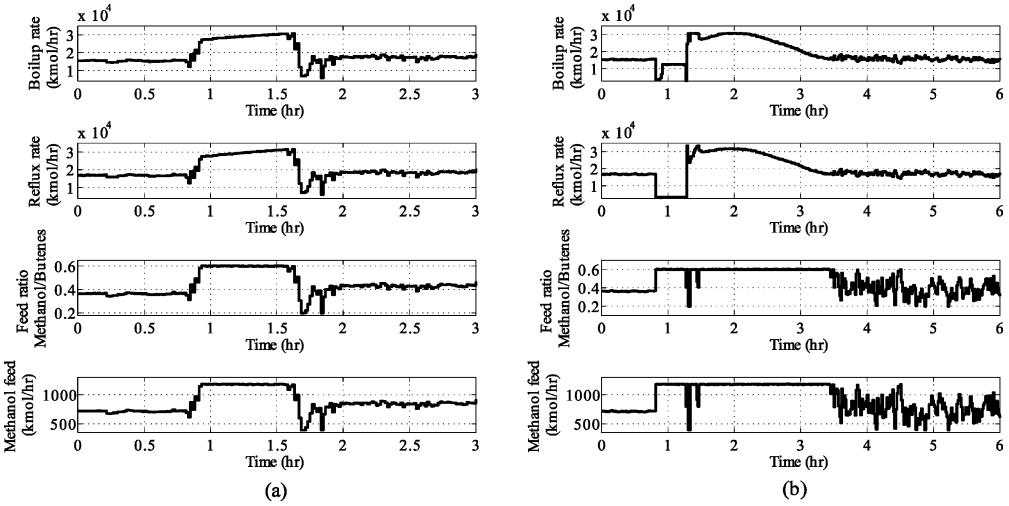

Figure 21. Profiles of manipulated inputs for the set-point tracking problem under stochastic conditions: (a) from the lower steady state to the middle steady state and (b) from the middle steady state to the upper steady state.

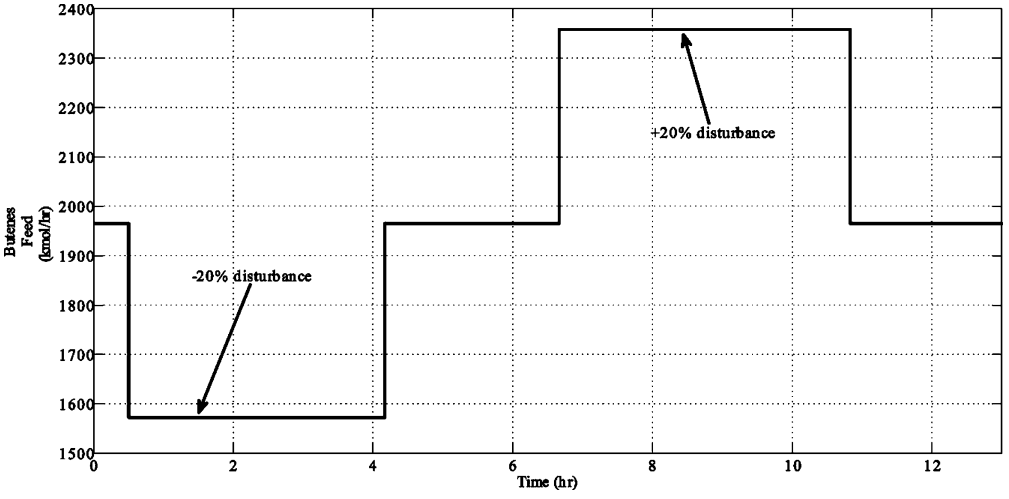

Figure 22. Feed rate disturbance (±20%) in the mix butene feed.

operating region. Moreover, these systems are, in general, stiff and are typically modeled as sets of differential-algebraic equations. These two factors render the control of RD systems a challenging problem, particularly when the desirable

dx.doi.org/10.1021/ie4004128 | Ind. Eng. Chem. Res. 2013, 52, 13699−13716

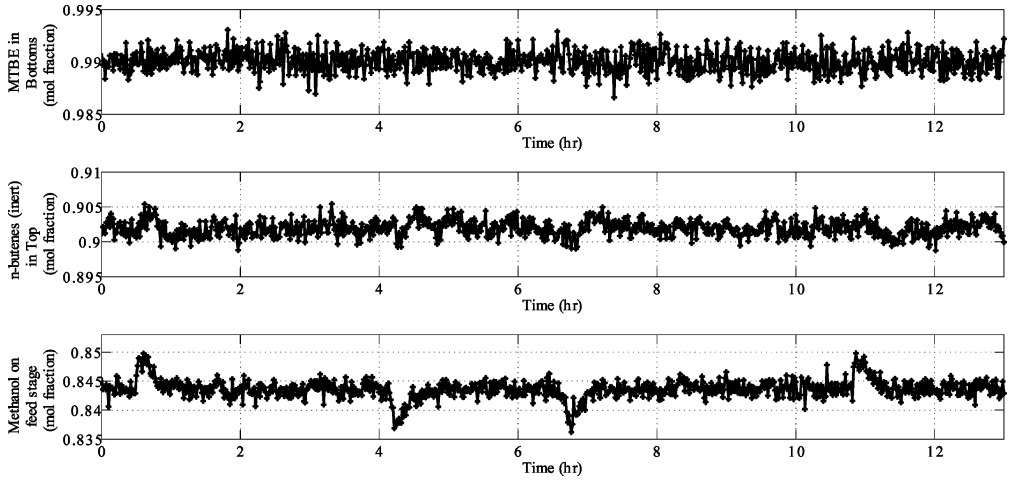

Figure 23. Profiles of controlled outputs for the disturbance rejection problem under stochastic conditions.

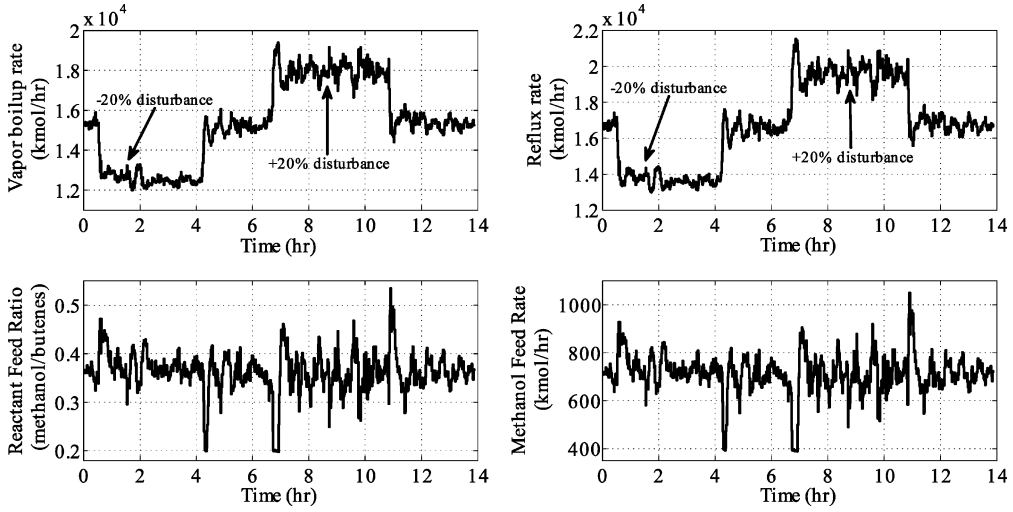

Figure 24. Profiles of manipulated inputs for the disturbance rejection problem under stochastic conditions.

operating point happens to be unstable. In this work, an observer error feedback-based NMPC scheme has been developed for achieving offset-free control of RD systems modeled as DAEs. A recently developed version of the EKF for DAE systems[29] was used to perform state estimations. Because direct use of DAE solvers in the NMPC formulation (referred to as ideal NMPC) can prove to be prohibitively computationally intensive and unsuitable for online implementation, a successive-linearization-based NMPC scheme was also developed. A significant advantage of the SLNMPC formulation is that it can be formulated as a QP problem.

To demonstrate the effectiveness of the proposed control schemes, control problems associated with two RD systems, namely, a hypothetical ideal RD column and an MTBE RD column, were investigated. The ideal RD column considered in the present work exhibits input and output multiplicities simultaneously. The economically desired steady state corresponds to an unstable operating point in the ideal RD column. Ideal NMPC and SLNMPC are expected to move the ideal RD column from the initial undesirable stable steady state to the desirable unstable steady state. Analysis of the simulation results indicates that, with the stoichiometric control configuration, both of the NMPC schemes were able to move the RD column effectively to the economically desired but unstable steady state. The NMPC schemes with the conventional control configuration, on the other hand, settled at the steady-state operating point corresponding to the higher values of manipulated inputs, which are economically less attractive. Moreover, SLNMPC was found to achieve closed-loop performance that was comparable to that of ideal NMPC at a significantly shorter computation time. Thus, the SLNMPC scheme with the stoichiometric control configuration was further investigated for the disturbance rejection problem and robustness against model−plant mismatch at the unstable steady state. Flow disturbances and model−plant mismatch of moderately large magnitudes were successfully rejected by SLNMPC with the stoichiometric control configuration.

The servo and regulatory performances of the proposed DAE-EKF-based SLNMPC scheme were further investigated on a real RD column involved in MTBE synthesis. As for the ideal RD system, an SLNMPC scheme was developed with a stoichiometric balance of the reactants in the reactive section. SLNMPC was able to manage the transition of the MTBE RD column from a low-purity initial point to a high-purity final operating point while stabilizing the system between the two extremes at an unstable operating point. The regulatory performance generated by the SLNMPC scheme was found to be qualitatively similar to that of the ideal RD system.

dx.doi.org/10.1021/ie4004128 | Ind. Eng. Chem. Res. 2013, 52, 13699−13716

Thus, the proposed SLNMPC formulation provides an effective approach for handling control problems involving moderately large-magnitude servo and regulatory changes in the operation of RD systems that exhibit input and output multiplicities. Moreover, the average computation time for the SLNMPC formulation was found to be significantly shorter than the sampling interval, which establishes the feasibility of implementing the SLNMPC scheme in real time.

AUTHOR INFORMATION

Corresponding Author

*E-mail: sachinp@iitb.ac.in.

Notes

The authors declare no competing financial interest.

REFERENCES

(1) Doherty, M. F.; Buzad, M. G. Reactive distillation by design. *Trans. Inst. Chem. Eng. A* **1992**, *70*, 448−458.

(2) Chen, F.; Huss, R. S.; Malone, M. F.; Doherty, M. F. Multiple steady states in reactive distillation: Kinetic effects. *Comput. Chem. Eng.* **2002**, *26*, 81−93.

(3) Engell, S.; Fernholz, G. Control of a reactive separation process. *Chem. Eng. Process.* **2003**, *42*, 201−210.

(4) Koppal, L. B. Input multiplicities in nonlinear multivariable control systems. *AIChE J.* **1982**, *28*, 935−945.

(5) Mohl, K.; Kienle, A.; Gilles, E.; Rapmund, P.; Sundmacher, K.; Hoffmann, U. Steady-state multiplicities in reactive distillation columns for the production of fuel ethers MTBE and TAME: Theoretical analysis and experimental verification. *Chem. Eng. Sci.* **1999**, *54* (8), 1029−1043.

(6) Singh, B. P.; Singh, R.; Kumar, M V. P.; Kaishtha, N. Steady state analysis of reactive distillation using homotopy continuation method. *Chem. Eng. Res. Des.* **2005**, *83A*, 959−968.

(7) Singh, A.; Tiwari, A.; Bansal, V.; Gudi, R. D.; Mahajani, S. M. Recovery of acetic acid by reactive distillation: Parametric study and nonlinear dynamic effects. *Ind. Eng. Chem. Res.* **2007**, *46*, 9196−9204.

(8) Morari, M. Robust stability of systems with integral control. In *Proceedings of the 22nd IEEE Conference on Decision and Control*; IEEE Press: Piscataway, NJ, 1983; pp 865−869.

(9) Srinivasrao, M.; Patwardhan, S. C.; Gudi, R. D. From data to nonlinear predictive control. 2. Improving regulatory performance using identified observers. *Ind. Eng. Chem. Res.* **2006**, *45*, 3593−3603.

(10) Al-Arfaj, M. A.; Luyben, W. L. Comparative control study of ideal and methyl acetate reactive distillation. *Chem. Eng. Sci.* **2002**, *57*, 5039−5050.

(11) Aris, R.; Amundson, N. R. Analysis of chemical reactors stability and control. *Chem. Eng. Sci.* **1958**, *7*, 121−155.

(12) Monroy-Loperena, R.; Perez-Cisneros, E.; Alvarez-Ramirez, J. A robust PI control configuration for a high-purity ethylene glycol reactive distillation column. *Chem. Eng. Sci.* **2000**, *55*, 4925−4937.

(13) Kumar, M. V. P.; Kaishtha, N. Steady state multiplicity and its implications on the control of an ideal reactive distillation column. *Ind. Eng. Chem. Res.* **2008**, *47*, 2778−2787.

(14) Volker, M.; Sonntag, C.; Engell, S. Control of integrated processes: A case study on reactive distillation in a medium-scale pilot plant. *Control Eng. Pract.* **2007**, *15*, 863−881.

(15) Kumar, A.; Daoutidis, P. Modeling, analysis and control of ethylene glycol reactive distillation column. *AIChE J.* **1999**, *32*, 459−465.

(16) Grüner, T. E.; Mohl, K. D.; Kienle, A., E. D.; Fernholz, G.; Friedrich, S. Nonlinear control of a reactive distillation column. *Control Eng. Pract.* **2003**, *11*, 915−925.

(17) Henson, M. A.; Seborg, D. E. An internal model control strategy for nonlinear systems. *AIChE J.* **1991**, *37* (7), 1065−1081.

(18) Qin, S. J.; Badgwell, T. A. A survey of industrial model predictive control technology. *Control Eng. Pract.* **2003**, *11* (7), 733.

(19) Kawathekar, R.; Riggs, J. B. Nonlinear model predictive control of a reactive distillation column. *Control Eng. Pract.* **2007**, *15*, 231−239.

(20) Venkateswarlu, Ch.; Reddy, A. D. Nonlinear model predictive control of reactive distillation based on stochastic optimization. *Ind. Eng. Chem. Res.* **2008**, *47* (18), 6949−6960.

(21) Diehl, M.; Bock, H. G.; Schlöder, J. P.; Findeisen, R.; Nagy, Z.; Allgöwer, F. Real time optimization and nonlinear model predictive control of processes governed by differential-algebraic equations. *J. Process Control* **2002**, *12*, 577−585.

(22) Schäfer, A.; Kühl, P.; Diehl, M.; Schlöder, J. P.; Bock, H. G. Fast reduced multiple shooting methods for nonlinear model predictive control. *Chem. Eng. Process.* **2007**, *46*, 1200−1214.

(23) Zavala, V. M.; Biegler, L. T. The advanced-step NMPC controller. *Automatica* **2009**, *45*, 86−93.

(24) Olanrewaju, M.; Al-Arfaj, M. A. Estimator-based control of reactive distillation system: Application of an extended Kalman filtering. *Chem. Eng. Sci.* **2006**, *61*, 3386−3399.

(25) Patwardhan, S. C.; Narasimhan, S.; Prakash, J.; Gopaluni, R. B.; Shah, S. L. Nonlinear Bayesian state estimation: Review and recent trends. *Control Eng. Pract.* **2012**, *20*, 933−953.

(26) Zavala, V. M.; Laird, C. D.; Biegler, L. T. A fast moving horizon estimation algorithm based on nonlinear programming sensitivity. *J. Process Control* **2008**, *18*, 876−884.

(27) Lo'pez-Negrete, R.; Patwardhan, S. C.; Biegler, L. T. Constrained particle filter approach to approximate the arrival cost in moving horizon estimation. *J. Process Control* **2011**, *21*, 909−919.

(28) Becerra, V. M.; Roberts, P. D.; Grifiths, G. W. Applying the extended Kalman filter to sytems described by nonlinear differential-algebraic equations. *Control Eng. Pract.* **2001**, *9*, 267−281.

(29) Mandela, R. K.; Rengaswamy, R.; Narasimhan, S. Recursive state estimation techniques for nonlinear differential algebraic systems. *Chem. Eng. Sci.* **2010**, *65*, 4548−4556.

(30) Huang, R., Patwardhan, S. C.; Biegler, L. T. Robust stability of nonlinear model predictive control with extended Kalman Filter and target setting. *Int. J. of Robust and Nonlinear Control* 2013, *23*, 1240−1264.

(31) Santos, L. O.; Afonso, P.; Castro, J.; Oliveira, N.; Biegler, L. T. On-line implementation of nonlinear MPC: An experimental case study. *Control Eng. Pract.* **2001**, *9* (8), 847−857.

(32) Chen, W.; Balance, D. J.; O'Reilly, J. Model predictive control of nonlinear systems: Computational burden and stability. *IEEE Proc. Control Theory Appl.* **2000**, *147* (4), 387−394.

(33) Brengel, D. D.; Seider, W. D. Multistep nonlinear predictive controller. *Ind. Eng. Chem. Res.* **1989**, *28*, 1812−1822.

(34) Al-Arfaj, M. A.; Luyben, W. L. Comparison of alternative control structures for an ideal two-product reactive distillation column. *Ind. Eng. Chem. Res.* **2000**, *39*, 3298−3307.

(35) Kumar, M. V. P.; Kaishtha, N. Internal heat integration and controllability of double feed reactive distillation columns, 1 effect of feed tray location. *Ind. Eng. Chem. Res.* **2008**, *47*, 7294−7303.

(36) Luyben, W. L. Economic and dynamic impact of the use of excess reactant in reactive distillation systems. *Ind. Eng. Chem. Res.* **2000**, *39*, 2935−2946.

(37) Sneesby, M. G.; Tadé, M. O.; Smith, T. N. Steady state transitions in the reactive distillation of MTBE. *Comput. Chem. Eng.* **1998**, *22* (No. 7−8), 879−892.

(38) Wang, S. J.; Wong, D. S. H.; Lee, E. K. Effect of interaction multiplicity on control system design for a MTBE reactive distillation column. *J. Process Control* **2003**, *13*, 503−515.

(39) Rehfinger, A.; Hoffman, U. Kinetics of methyl tertiary butyl ether liquid phase synthesis catalyzed by ion exchange resin - I. Instrinsic rate expression in liquid phase activities. *Chem. Eng. Sci.* **1990**, *45* (6), 1605−1617.

(40) Luyben, W. L.; Yu, C. C. Control of MTBE and ETBE Reactive Distillation Columns. In *Reactive Distillation Design and Control*; John Wiley & Sons: New York, 2008; pp 407−428.